THE
PHYSICAL REVIEW

A journal of experimental and theoretical physics established by E. L. Nichols in 1893

SECOND SERIES, VOL. 143, NO. 1 4 MARCH 1966

Multiphoton Ionization of Hydrogen and Rare-Gas Atoms*†

H. BARRY BEBB‡ AND ALBERT GOLD
Institute of Optics, University of Rochester, Rochester, New York
(Received 8 October 1965)

A perturbation theory of the ionization of atoms by simultaneous absorption of several photons, each of whose energy is less than the ionization potential, is developed from the evolution-operator formalism. A precise computation is made for the hydrogen atom, giving transition rates as a function of photon energy for two- through twelve-photon photoionization. The eighth-order ionization rate (in cgs units) at the 1.78-eV ruby-laser line is found to be $\sim 10^{-244} \times$ (photon flux)^8 and should be observable using available techniques. Good agreement is obtained with Zernik's exact calcualtion of the two-photon ionization rate of metastable $2S$ hydrogen. Approximate calculations are made for the rare gases. Assuming "typical" experimental conditions of a gas density of $\sim 10^{20}$ atoms cm^{-3} and a ruby laser focused into a volume of $\sim 10^{-8}$ cm^3, we find that the flux required to liberate one electron during a 10-nsec pulse is $\sim 10^{29}$ cm^{-2} sec^{-1} for Xe, Kr, and Ar and $\sim 5 \times 10^{30}$ photons cm^{-2} sec^{-1} for Ne and He. These gases ionize with the simultaneous absorption of 7, 8, 9, 13, and 14 photons, respectively. The predicted rate for Xe is found to be in excellent agreement with the recent direct measurements of Voronov and Delone. We conclude that multiphoton ionization provides the initial electrons required for the optical breakdown of gases, though it does not account for the over-all growth of the discharge except possibly at very low pressures. Impurity atoms (particularly heavy rare gases) may be the source of "initiating" electrons in Ne and He.

I. INTRODUCTION

THE breakdown of various gases in the focal region of a Q-switched laser has been reported by several workers.[1–4] The growth of optical discharges in rare gases seems to be quite well accounted for by inverse-bremsstrahlung theory which gives results very close to those obtained through the *ad hoc* use of the classical theory of microwave breakdown.[5] The cascading ionization is found to take place through the agency of "free" electrons absorbing energy from the field while in the neighborhood of gas atoms. There thus remains the query, "Whence the initial electron(s) which trigger the breakdown?" We assert that they are provided by direct multiphoton ionization of neutral gas atoms, cautioning, however, that in some instances the ionization of impurity atoms present in minute concentrations may play a dominant role.

The advent of the laser has led to abundant experimental verification[6–10] of Goeppert-Mayers' theory[11] of the simultaneous absorption of two photons by an atomic system. This new experimental capability has in turn motivated application of the theory to a variety of specific systems.[12–17] In particular, Zernik[16] has per-

* Research supported in part by a contract with the U. S. Army Research Office—Durham and in part by a grant from the National Science Foundation.

† A summary of some of the results of this work was presented at the Physics of Quantum Electronics Conference, San Juan, Puerto Rico, 1965.

‡ National Aeronautics and Space Agency predoctoral fellow. This work is based in part on a thesis submitted in partial fulfillment of the requirements for the Degree of Doctor of Philosophy.

[1] R. G. Meyerand and A. F. Haught, Phys. Rev. Letters **11**, 401 (1963); **13**, 7 (1964).

[2] R. W. Minck, J. Appl. Phys. **35**, 252 (1964).

[3] R. G. Tomlinson, Phys. Rev. Letters **14**, 489 (1965).

[4] R. W. Waynant and J. H. Ramsay, report read at the Spring Meeting of the Optical Society of America, Dallas, 1965 (unpublished).

[5] A. V. Phelps, *Proceedings of the Physics of Quantum Electronics Conference at San Juan, Puerto Rico* (McGraw-Hill Book Company, Inc., New York, to be published). See also J. K. Wright, Proc. Phys. Soc. (London) **84**, 41 (1964).

[6] W. Kaiser and C. G. Garrett, Phys. Rev. Letters **7**, 229 (1961).

[7] I. D. Abella, Phys. Rev. Letters **9**, 453 (1962).

[8] W. L. Peticolas, J. P. Goldsborough, and K. E. Reickhoff, Phys. Rev. Letters **10**, 43 (1963).

[9] J. A. Giordmaine and J. H. Howe, Phys. Rev. Letters **11**, 207 (1963).

[10] R. Braunstein and N. Ockman, Phys. Rev. **134**, A499 (1964).

[11] M. Goeppert-Mayer, Ann. Physik **9**, 273 (1931).

[12] R. Braunstein, Phys. Rev. **125**, 475 (1962).

[13] R. Loudon, Proc. Phys. Soc. **80**, 952 (1962).

[14] J. D. Axe, Phys. Rev. **136**, A42 (1964).

[15] A. Gold and J. Hernandez, Phys. Rev. **139**, A2002 (1965).

[16] W. Zernik, Phys. Rev. **135**, A51 (1964); W. Zernik and R. W. Klopfenstein, J. Math Phys. **6**, 262 (1965).

[17] S. Geltman, Phys. Letters **4**, 168 (1963).

formed an exact calculation of the two-photon ionization rate of metastable $2S$ hydrogen atoms and Geltman[17] has made an estimate of the two-photon photodetachment of negative halide ions. The latter is in quite reasonable agreement with the measurements of Hall, Robinson, and Branscomb.[18] The present authors have extended the perturbation-theory treatment to the computation of N-photon photo-ionization rates for rare-gas atoms, using rather crude approximate wave functions and matrix elements.[19] Keldysh has written a semiclassical theory of multiphoton ionization.[20] He extends Oppenheimer's[21] perturbation theory of tunneling in static fields to the optical-frequency regime. Voronov and Delone have measured the rate of ionization of Xe atoms by ruby-laser light.[22] Their results are in good agreement with our calculation's prediction for this seven-photon process.

In this paper we carry out a precise, detailed calculation of the N-photon ionization rate of atomic hydrogen for $N=2$ to 12. ($N=8$ for the ruby laser.) The general features of and insights gained from this calculation are then applied to the rare gases Xe, Kr, Ar, Ne, and He, whose ionizations require 7, 8, 9, 13, and 14 ruby laser photons, respectively. All rates calculated are high enough to be measured using presently available lasers.[23] The rare-gas results indicate that direct multiphoton ionization provides the initiating electron(s) for the observed optical breakdown of Xe, Kr, and Ar, while it seems likely that very small traces of impurities, particularly heavier rare gases, furnish the first electrons in Ne and He.

Section II presents the formal theory of multiphoton ionization. The evolution operator technique is used to treat the interaction of the quantized field with the atomic system. Expressions are developed for the lowest order contributions to transitions involving absorption of N photons. Explicit formulas for multiphoton ionization are then written. These results are applied to a precise perturbation calculation of the multiphoton ionization rate of hydrogen in Sec. III. Coulomb final states are used and summations over intermediate states are carefully performed. Section IV contains a much more approximate computation of transition rates and "initiation" fluxes for the rare gases Xe, Kr, Ar, Ne, He. The calculation is based on a "hydrogenic" model. Results are discussed in Sec. V. Comparison to observed cross sections is made. The relationship of multiphoton ionization to optical breakdown in the rare gases is considered. The role of the mode structure of the exciting laser beam on the interpretation of experimental data is also briefly examined. Appendix A derives selection rules for multiphoton transitions in the hydrogen atom. Appendix B presents the details of the calculation of the hydrogen "average energy denominators" which appear in high-order matrix elements.

[18] J. L. Hall, E. J. Robinson, and L. M. Branscomb, Phys. Rev. Letters **14**, 1013 (1965).
[19] A. Gold and H. B. Bebb, Phys. Rev. Letters **14**, 60 (1965).
[20] L. V. Keldysh, Zh. Eksperim. i Teor. Fiz. **47**, 1945 (1964) [English transl.: Soviet Phys.—JETP **20**, 1307 (1965)].
[21] J. R. Oppenheimer, Phys. Rev. **31**, 66 (1928).
[22] G. S. Voronov and N. B. Delone, Zh. Eksperim. i Teor. Fiz. Pis'ma Red. **1**, 66 (1965) [English transl.: Soviet Phys.—JETP Letters **1**, 66 (1965)].
[23] Multiple-photon ionization experiments can probably be most effectively performed using atomic-beam techniques similar to those reported in Ref. 18.

II. FORMAL THEORY

1. Perturbation Expansion

Power and Zienau[24] have shown that the Hamiltonian for a bound electron interacting with a radiation field can be written

$$H=H_0+H_I, \tag{1a}$$

where

$$H_I=-e\mathcal{E}(\mathbf{r},t)\cdot\mathbf{r} \tag{1b}$$

$$H_0=H_e+H_r \tag{1c}$$

and

$$H_e=\mathbf{p}^2/2m+V(\mathbf{r}) \tag{1d}$$

$$H_r=(1/8\pi)\int|\mathcal{E}|^2+|\mathcal{H}|^2dV=\sum_\lambda \eta_\lambda\hbar\omega_\lambda. \tag{1e}$$

In Eqs. (1), $\mathcal{E}(\mathbf{r},t)$ is the transverse part of the electric field. (The Coulomb gauge has been assumed.) The second equality of (1e) presupposes quantization of the radiation field; η_λ denotes the number operator for mode λ.

The use of the quantum-electrodynamic formalism is convenient (though not necessary) for considering optical maser sources. Following Heitler[25] (whose notation we adopt) we define the electric field operator in terms of annihilation and creation operators, q_λ and $q_\lambda^\dagger$,

$$\mathcal{E}=(i/c)\textstyle\sum_\lambda(\omega_\lambda q_\lambda\mathbf{A}_\lambda-\omega_\lambda q_\lambda^\dagger\mathbf{A}_\lambda^*), \tag{2a}$$

where

$$\mathbf{A}_\lambda=(4\pi c^2)^{1/2}e^{i\mathbf{k}_\lambda\cdot\mathbf{r}}\boldsymbol{\varepsilon}. \tag{2b}$$

The "ladder" operators are defined by

$$q_\lambda|n_\lambda\rangle=[(\hbar/2\omega_\lambda)n_\lambda]^{1/2}|n_\lambda-1\rangle, \tag{3a}$$

$$q_\lambda^\dagger|n_\lambda\rangle=[(\hbar/2\omega_\lambda)(n_\lambda+1)]^{1/2}|n_\lambda+1\rangle. \tag{3b}$$

The state $|n_\lambda\rangle$ of the radiation field is specified by the photon occupation number, n_λ. The complete radiation field is described by specifying the entire set of occupation numbers over all modes, $|n_1,n_2,\cdots,n_\lambda,\cdots\rangle$. These states are the eigenstates of H_r (or the number operator),

$$H_r=\textstyle\sum_\lambda\eta_\lambda\hbar\omega_\lambda=\sum_\lambda[(2\omega_\lambda/\hbar)q_\lambda^\dagger q_\lambda]\hbar\omega_\lambda. \tag{4}$$

In (4), the number operator is implicitly defined in terms of the "ladder" operators.

[24] E. A. Power and S. Zienau, Phil. Trans. Roy. Soc. (London) **A251**, 427 (1959); Nuovo Cimento **6**, 7 (1957).
[25] W. Heitler, *The Quantum Theory of Radiation* (Oxford University Press, London, 1954).

We develop the theory of multiple-photon absorption by direct application of time-dependent perturbation theory using the concept of evolution operators. Since evolution operators are only occasionally used in atomic or solid-state physics, we give a brief resume of their properties.[26] Within the interaction representation, the time evolution of the system arises solely from the interaction part of the Hamiltonian. Suppose that at time $t'=0$, the system is in one of the eigenstates $|g\rangle$ of the unperturbed Hamiltonian, H_0. Then after time t, the state of the system is $|\psi(t)\rangle$. We postulate that there exists an (evolution) operator $U_I(t)$ such that $|\psi(t)\rangle = U_I(t)|g\rangle$. The probability amplitude b_n that the system is in some other eigenstate of H_0, say $|n\rangle$, is clearly given by the projection of $|\psi(t)\rangle$ on to $|n\rangle$,

$$b_n=\langle n|\psi(t)\rangle=\langle n|U_I(t)|g\rangle.$$

If $|\psi(t)\rangle$ is represented in terms of the complete set of orthonormal eigenstates of H_0, then b_n, is just one of the expansion coefficients of

$$|\psi(t)\rangle=\textstyle\sum_m b_m(t)|m\rangle.$$

Thus, by definition, the probability that the system has undergone a transition from $|g\rangle$ to $|n\rangle$ in time t is

$$W_{n,g}(t)=|\langle n|U_I(t)|g\rangle|^2=|b_n|^2 \tag{5}$$

and the transition probability per unit time is

$$w_{n,g}=(d/dt)W_{n,g}(t). \tag{6}$$

Since the evolution operator satisfies Schrödinger's equation, we may write

$$U_I(t)=1+(i\hbar)^{-1}\int^t H_I'(t')U_I(t')dt'$$

which is just the integral form for Schrödinger's equation (in the interaction representation) with $H_I'(t)$ given by

$$H_I'(t)=e^{iH_0t/\hbar}H_Ie^{-iH_0t/\hbar}.$$

By successively substituting the right-hand side of this expression back in for $U_I(t')$, we arrive at

$$U_I(t)=1+\sum_{n=1}^{\infty}U_I^{(n)}(t), \tag{7a}$$

where

$$\begin{aligned}U_I^{(n)}(t)&=(i\hbar)^{-n}\int_0^t dt_n\int^{t_n}dt_{n-1}\cdots\int^{t_2}dt_1H_I'(t_n)H_I'(t_{n-1})\cdots H_I'(t_1)\\&=(i\hbar)^{-n}\int^t d^nt\,H_I'(t_n)H_I'(t_{n-1})\cdots H_I'(t_1).\end{aligned} \tag{7b}$$

To calculate the Nth-order contribution to the transition rate between, say the ground state $|g\rangle$ and some final state $|f\rangle$, we must determine the matrix element of $U_I^{(N)}(t)$. From the definition of $U_I^{(N)}(t)$ given by Eq. (7b), we have

$$\begin{aligned}\langle f|U_I^{(N)}(t)|g\rangle&=(i\hbar)^{-N}\int_0^t d^Nt\langle f|H_I'(t_N)H_I'(t_{N-1})\cdots H_I'(t_2)H_I'(t_1)|g\rangle\\&=(i\hbar)^{-N}\int_0^t d^Nt\sum_{m_{N-1}}\sum_{m_{N-2}}\cdots\sum_{m_2}\sum_{m_1}\langle f|H_I'(t_N)|m_{N-1}\rangle\\&\quad\times\langle m_{N-1}|H_I'(t_{N-1})|m_{N-2}\rangle\cdots\langle m_2|H_I'(t_2)|m_1\rangle\langle m_1|H_I'(t_1)|g\rangle.\end{aligned} \tag{8}$$

The sums over the m_ν are extended over the complete set of states of H_0, discrete plus continuum. Next we integrate over time. To eliminate rapidly oscillating terms, the lower limits on the intermediate integrals are taken as $t'\to\infty$.[27] The lower limit on the final integral is taken at $t=0$ to ensure the final state was not occupied before the perturbation was "turned on." Thus,

$$\langle f|U_I^{(N)}(t)|g\rangle=(-\hbar)^{-N}\frac{e^{i\omega_{fg}t}-1}{\omega_{f,g}}M_{f,g}^{(N)}, \tag{9a}$$

where

$$M_{f,g}^{(N)}=\sum_{m_{N-1}}\sum_{m_{N-2}}\cdots\sum_{m_2}\sum_{m_1}\langle f|H_I|m_{N-1}\rangle\frac{\langle m_{N-1}|H_I|m_{N-2}\rangle}{\omega_{m_{N-1},g}}\times\frac{\langle m_{N-2}|H_I|m_{N-3}\rangle}{\omega_{m_{N-2},g}}\times\cdots\times\frac{\langle m_1|H_I|g\rangle}{\omega_{m_1,g}}. \tag{9b}$$

[26] For an extensive treatment, see A. Messiah, *Quantum Mechanics* (John Wiley & Sons, Inc., New York, 1962), Vols. I & II.

[27] See Ref. 25, p. 140.

The frequencies appearing in Eqs. (9) are defined in the usual manner, $\omega_{k,l}=(E_k-E_l)/\hbar$, where E_k and E_l are the eigenenergies of the unperturbed Hamiltonian H_0; these energies include both radiation field and the atomic energies.

So far the formulas derived are quite general and applicable to a large class of multiple-photon effects. We now specify that we are concerned with N-photon photoionization. Obviously, the lowest order contribution to photoionization cannot involve the creation of photons. Therefore, the only part of the field operator $\mathcal{E}$ that requires consideration is

$$\mathcal{E}=(i/c)\sum_\lambda \omega_\lambda q_\lambda \mathbf{A}_\lambda, \tag{10}$$

where q_λ is the annihilation operator defined in Eq. (3a) and $\mathbf{A}_\lambda$ is given by Eq. (2b). For simplicity of notation we consider a radiation field containing only one mode of frequency ω and occupation number n. With these considerations, we take the interaction Hamiltonian, H_I, as

$$H_I=-e\mathcal{E}\cdot\mathbf{r}=(-ie/c)\omega q\mathbf{A}\cdot\mathbf{r}=-ieR(4\pi)^{1/2}\omega q. \tag{11}$$

The new quantity $R(=e^{i\mathbf{k}\cdot\mathbf{r}}\boldsymbol{\varepsilon}\cdot\mathbf{r})$ operates only on atomic states.

The matrix elements of H_I can immediately be evaluated. Let the state $|g\rangle$ be denoted $|a_g;n\rangle$, where a_g specifies the atomic quantum numbers and n specifies occupation number of the field. Similarly the states $|m_\nu\rangle$ are represented by $|a_\nu;n'\rangle$. Using the definition (3a) for the annihilation operator q and recalling that for each successive matrix element the radiation field is depleted by one photon, the Nth order matrix element $M_{f,g}^{(N)}$ defined by Eq. (9b), becomes

$$M_{f,g}^{(N)}=[-ie(2\pi\hbar\omega)^{1/2}]^N\{[n-(N-1)]\times[n-(N-2)]\times\cdots\times[n-1][n]\}^{1/2}K_{af,a_g}^{(N)}, \tag{12}$$

where

$$K_{af,a_g}^{(N)}=\sum_{aN-1}\sum_{aN-2}\cdots\sum_{a_2}\sum_{a_1}\langle a_f|R|a_{N-1}\rangle\times\frac{\langle a_{N-1}|R|a_{N-2}\rangle}{(\omega_{aN-1,a_g}-(N-1)\omega)}\times\cdots\times\frac{\langle a_1|R|a_g\rangle}{(\omega_{a1,a_g}-\omega)}. \tag{13}$$

In (13) we have separated the frequencies appearing in the denominator of Eq. (9b) into the atomic and field frequencies,

$$\omega_{m_1,g}=\omega_{m_1}-\omega_g=[\omega_{a_1}+(n-1)\omega]-[\omega_{a_g}-n\omega]=\omega_{a_1,a_g}-\omega.$$

Putting the results into Eq. (5) gives

$$W_{f,g}^{(N)}(t)=|\langle f|U_I^{(N)}(t)|g\rangle|^2=\hbar^{-2N}f(\omega_{f,g},t)|M_{f,g}^{(N)}|^2=[2\pi(e^2/\hbar)\omega n]^N f(\omega_{f,g},t)|K_{af,a_g}|^2, \tag{14}$$

where $K_{af,a_g}^{(N)}$ is given by Eq. (13) and

$$f(\omega_{f,g},t)=|(e^{i\omega_{f,g}t}-1)/\omega_{f,g}|^2.$$

We have neglected the depletion of the photon field in the last line of Eq. (14). This is reasonable for optical-maser sources since the occupation number is of the order of 10^{20}.

It is convenient to replace n by F/c where F (No. photons cm^{-2} sec^{-1}) is the photon flux. Further, since we are interested in times long compared to $1/\omega_{f,g}$ we replace $f(\omega,t)$ by its asymptotic value, $2\pi t\delta(\omega)$. Then, the transition rate per atom can be written

$$(d/dt)W_{f,g}^{(N)}(t)=2\pi(2\pi\alpha F\omega)^N\times|K_{af,a_g}^{(N)}|^2\delta(\omega_{f,g}), \tag{15}$$

where α is the fine structure constant, $e^2/\hbar c$. Equation (15) is useful for considering transitions between two discrete atomic states.

When the transitions are to the continuum, one must treat a group of neighboring states within a small energy range $d\epsilon_{f,g}$ rather than a single state. From Eq. (15) we have, upon integration over $\epsilon_{f,g}$ [incorporating the appropriate density of states, $\rho(\epsilon_{f,g})$],

$$w_{f,g}^{(N)}=2\pi\hbar(2\pi\alpha F\omega)^N|K_{af,a_g}^{(N)}|^2\rho(0). \tag{16}$$

The density of final states, ρ, depends on the normalization of the continuum-state functions.[28] In this work the continuum-state wave functions are normalized so that $\rho(\mathbf{k})=(2\pi)^{-3}$. Then, the density of states with respect to energy becomes

$$\rho(\epsilon)=\frac{(m/\hbar^2)k}{(2\pi)^3}d\Omega_k,$$

where k is the wave number of the electron and the energy is defined by

$$\epsilon_{f,g}=\epsilon_I-N\hbar\omega+\hbar^2k^2/2m=0.$$

ϵ_I is the ionization energy of the atom, $\hbar\omega$ is the photon energy, and the last term is the kinetic energy of the electron. Substituting the density of states into (16) gives

$$w_{f,g}^{(N)}(\theta_k,\phi_k)=\frac{m/\hbar}{(2\pi)^2}(2\pi\alpha F\omega)^N|K_{af,a_g}^{(N)}|^2k. \tag{17}$$

Here, $w_{f,g}^{(N)}(\theta_k,\phi_k)$ denotes the "differential" transition rate corresponding to the probability for emission of an electron in the direction (θ_k,ϕ_k) within the solid angle $d\Omega_k$. The total transition rate per atom is

$$w_{f,g}^{(N)}=\int d\Omega_k w_{f,g}^{(N)}(\theta_k,\phi_k). \tag{18}$$

[28] See Ref. 26, Vol. I, p. 170.

Equation (17) is the central result of this section. The integral over $d\Omega_k$ cannot be performed until the final-state wave function has been more fully specified.

The Nth-order contribution to the perturbation expansion for the transition rate can be written in the form

$$w_{f,g}^{(N)}=\text{const}(0.85\times10^{-33}F\hbar\omega)^N|K_{af,ag}|^2k,$$

where $\hbar\omega$ is the laser photon energy measured in electron volts, the number in the bracket is just a combination of natural constants, and other symbols are as previously defined. The convenience of the expansion and the adequacy of keeping only the lowest nonvanishing term follows from the quantity in parentheses. The $K_{af,ag}^{(N)}$ (with matrix elements in atomic units and energy denominators in electron volt) vary but slowly with N. Hence, conservatively speaking, the present perturbation treatment should suffice for fluxes $\lesssim10^{33}$, higher order contributions being negligible. However, for very strong intermediate resonances saturation of the intermediate state may place a lower limit on the validity of perturbation theory.[16] The typical fluxes encountered in breakdown experiments are $F\sim10^{29}-10^{31}$ photons cm^{-2} sec^{-1}.

2. Damping and Level Shifts

A rigorous treatment of damping and level shifts is difficult even for "one-photon" problems and is an unexplored area in multiple-photon effects. Although detailed discussion is beyond the scope of the present paper a phenomenological damping term can be put into the theory following Weisskopf and Wigner.[29] They assume initial- and final-state wave functions with time dependence

$$|\psi_a(t)\rangle=e^{-i\omega_at-\gamma_at/2}|a\rangle.$$

The principal consequence is an addition of a $\frac{1}{2}i\gamma$ to every energy denominator appearing in our equations, where γ is the combined width of initial and final states.

Detailed treatment reveals a complex, flux-dependent damping parameter $\gamma'+i\gamma''$ causing both a shift[30] and broadening[16] of the resonance lines. With the photon fluxes available from optical maser sources, the shift of lines and even the ionization edge may sometimes be significant. (Order of magnitude estimates place the shifts in the tantalizing region of ~0.1 eV.) We reserve further discussions of damping. Henceforth, we shall include it in our energy denominators when it is important and omit it otherwise. This slight looseness in usage should cause no confusion.

3. Notation

Because of the complexity of the Nth-order matrix elements it is convenient to develop an abbreviated notation. We associate a transition operator T_ν with each sum over states:

$$T_\nu=\sum_{a_\nu}\frac{R|a_\nu\rangle\langle a_\nu|}{(\omega_{a_\nu,a_g}-\nu\omega+i\gamma/2)}. \tag{19}$$

We also define τ^m as

$$\tau^m=[\prod_{\nu=1}^{m-1}T_\nu]R. \tag{20}$$

The Nth-order matrix element, (13), is now written in terms of the Nth-order transition operator,

$$K_{af,ag}^{(N)}=\langle a_f|\tau^{(N)}|a_g\rangle. \tag{21}$$

If we wish to separate out the $(N-1)$th order, we write

$$K_{af,ag}^{(N)}=\langle a_f|T_{N-1}\tau^{N-1}|a_g\rangle$$
$$=\sum_{aN-1}\frac{\langle a_f|R|a_{N-1}\rangle}{(\omega_{aN-1,ag}-(N-1)\omega+i\gamma/2)}\times\langle a_{N-1}|\tau^{N-1}|a_g\rangle. \tag{22}$$

Only the portion of the matrix element of interest need be explicitly displayed.

4. Evaluation of Nth-Order Matrix Elements

The chief difficulty in calculating the transition probability for N-photon ionization is the evaluation of the Nth-order matrix element $K_{af,ag}^{(N)}$. Perhaps its most conspicuous feature is the appearance of many infinite summations over electronic eigenstates. The energy denominators associated with these summations over intermediate states can, under fortuitous circumstances, become small. If, say in νth order, $\nu\omega$ is nearly equal to one of the atomic energies, then that atomic state will make the dominant contribution to the sum.[19] These "near resonances" are the key to making approximate calculations of the matrix elements. The "near resonances" also cause a characteristic dispersion in the transition probability as a function of the photon energy.

For simplicity of notation, we immediately make the dipole approximation and assume the radiation field is polarized in the z direction, then,

$$R=e^{i\mathbf{k}\cdot\mathbf{r}}\boldsymbol{\varepsilon}\cdot\mathbf{r}=z. \tag{23}$$

With this simplification the Nth-order matrix element (13) is given by

$$K_{af,ag}^{(N)}=\sum_{aN-1}\sum_{aN-2}\cdots\sum_{a2}\sum_{a1}\langle a_f|z|a_{N-1}\rangle\times\frac{\langle a_{N-1}|z|a_{N-2}\rangle}{(\omega_{aN-1,ag}-(N-1)\omega+i\gamma/2)}\times\frac{\langle a_{N-2}|z|a_{N-3}\rangle}{(\omega_{aN-2,ag}-(N-2)\omega+i\gamma/2)}\times\cdots\times\frac{\langle a_1|z|a_g\rangle}{(\omega_{a1,ag}-\omega+i\gamma/2)}, \tag{24}$$

[29] V. F. Weisskopf and E. P. Wigner, Z. Physik **63**, 54 (1930); **65**, 18 (1930).

[30] M. Mizushima, Phys. Rev. **133**, A414 (1964).

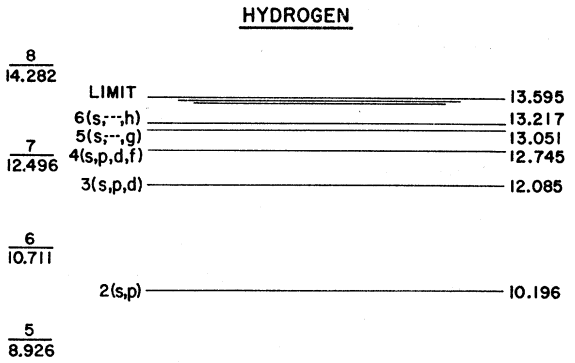

FIG. 1. Relevant portion of the hydrogen spectrum. All energies are in electron volts. Integral multiples of the ruby-laser photon energy (1.785 eV) are also indicated.

where the "sums" extend over complete sets of atomic eigenstates, $|a_\nu\rangle$.

We eliminate the "sums" by using an "average" frequency,[19] $\bar{\omega}(\nu)$, independent of the state, to replace the atomic frequencies ω_{a_ν,a_g}. Then, the numerator of Eq. (24) can be "collapsed" to give

$$K_{af,ag}{}^{(N)}=\frac{\langle a_f|z^N|a_g\rangle}{\prod_{\nu=1}^{N-1}[\bar{\omega}(\nu)-\nu\omega+i\gamma/2]}. \tag{25}$$

The equal sign is retained in (25) since there must exist some set of frequencies $\bar{\omega}(\nu)$ such that the two matrix elements are equal. No approximations are yet involved. In fact, a little algebra reveals that the "average" frequencies are defined (neglecting damping) by,

$$\sum_{a_\nu}\frac{\langle a_f|z^{N-\nu}|a_\nu\rangle\langle a_\nu|z^\nu|a_g\rangle}{(\omega_{a_\nu,a_g}-\nu\omega)}=\frac{\langle a_f|z^N|a_g\rangle}{[\bar{\omega}(\nu)-\nu\omega]}. \tag{26}$$

This result is obtained by defining $\bar{\omega}(\mu)$ in each successive order μ by equating the right-hand sides of (24) and (25).

Additional reduction of Eq. (25) is possible by assuming there exists a single "average" frequency for the virtual states, $\bar{\omega}_v$, independent of the order, ν. The new "average" frequency is

$$\prod_{\nu=1}^{N-1}[\bar{\omega}(\nu)-\nu\omega]=\prod_{\nu=1}^{N-1}(\bar{\omega}_v-\nu\omega). \tag{27}$$

The Nth-order matrix element then becomes

$$K_{af,ag}{}^{(N)}=\frac{\langle a_f|z^N|a_g\rangle}{\prod_{\nu=1}^{N-1}(\bar{\omega}_v-\nu\omega+\frac{1}{2}i\gamma)}. \tag{28}$$

In this form the problem of evaluating an Nth-order matrix element is reduced to determining an "average frequency," which in principle is well defined by Eqs. (26) and (27) and calculating a single matrix element. Of course, a straightforward evaluation of $\bar{\omega}_v$ still involves an infinite sum (see Appendix B). From a purely formal point of view, the number of matrix elements to be evaluated has been greatly reduced and we have therefore made progress. In addition the occurrence of "near resonances" can be used to simplify the calculations.

The electronic spectrum of atomic hydrogen is shown in Fig. 1. Integral multiples of the photon energy of a ruby laser (1.785 eV) measured from the ground state are also indicated. It will be seen that the $n=4$ state of hydrogen falls within 0.25 eV of being seven photon energies above the ground state. Owing to this "near resonance," we expect the $n=4$ state to make a dominant contribution to the sum over states. To make use of such coincidences, we avoid "collapsing" the matrix element on the sum containing the near resonance. If, the near resonance occurs in only one order, say ν, we take the matrix element (24) to be

$$\begin{aligned}K_{af,ag}{}^{(N)}&=\sum_{a_\nu}\frac{\langle a_f|z^{N-\nu}|a_\nu\rangle\langle a_\nu|z^\nu|a_g\rangle}{(\omega_{a_\nu,a_g}-\nu\omega+i\gamma/2)\prod_{\substack{\mu=1\\\mu\neq\nu}}^{N-1}[\bar{\omega}_\nu(\mu)-\mu\omega+i\gamma/2]}\\&=\frac{1}{\prod_{\substack{\mu=1\\\mu\neq\nu}}^{N-1}(\bar{\omega}_v-\mu\omega+i\gamma/2)}\sum_{a_\nu}\frac{\langle a_f|z^{N-\nu}|a_\nu\rangle\langle a_\nu|z^\nu|a_g\rangle}{(\omega_{a_\nu,a_g}-\nu\omega+i\gamma/2)},\end{aligned} \tag{29}$$

where we have added the subscript ν to the average frequency $\bar{\omega}_\nu(\mu)$ to remind us that its value depends on the states a_ν. Unless $\nu=N-1$, two equations are required to define $\bar{\omega}_\nu(\mu)$, one for $\mu>\nu$ and one for $\mu<\nu$:

$$\sum_{\substack{a_\mu\\\mu>\nu}}\frac{\langle a_f|z^{N-\nu-\mu}|a_\mu\rangle\langle a_\mu|z^\mu|a_\nu\rangle}{(\omega_{a_\mu,a_g}-\mu\omega)}=\frac{\langle a_f|z^{N-\nu}|a_\nu\rangle}{[\bar{\omega}_\nu(\mu)-\mu\omega]}, \tag{30}$$

and

$$\sum_{\substack{a_\mu\\\mu<\nu}}\frac{\langle a_\nu|z^{\nu-\mu}|a_\mu\rangle\langle a_\mu|z^\mu|a_g\rangle}{(\omega_{a_\mu,a_g}-\mu\omega)}=\frac{\langle a_\nu|z^\nu|a_g\rangle}{[\bar{\omega}_\nu(\mu)-\mu\omega]}. \tag{31}$$

The final average $\bar{\omega}_v$ is defined in analogy with Eq. (27),

$$\prod_{\substack{\mu=1\\\mu\neq\nu}}^{N-1}[\bar{\omega}_\nu(\mu)-\mu\omega]=\prod_{\substack{\mu=1\\\mu\neq\nu}}^{N-1}(\bar{\omega}_v-\mu\omega). \tag{32}$$

The extension to additional "near resonances" is obvious.[19]

Strictly speaking, $\bar{\omega}_v$ depends on the state a_ν as well as a_f, a_g and the photon energy and finally the order N, of the matrix element. Thus $\bar{\omega}_v$ must in principle be evaluated for each term of the indicated summation in

Eq. (29). What we hope, and indeed find, is that $\bar{\omega}_v$ does not depend strongly on the parameters and can therefore, to a good approximation, be replaced by some fixed value. Direct computations for hydrogen, which are outlined in Appendix B, set this value near the first excited level which possesses nonvanishing matrix elements coupling to the ground state, i.e., for H, $\epsilon_{2p,1s}=10.2$ eV. For more complicated atomic systems, we cannot perform the direct computations required to define $\bar{\omega}_v$; hence, we simply choose $\bar{\omega}_v$ as the first excitation level in analogy with hydrogen. This choice of $\bar{\omega}_v$ differs from the value assumed by Gold and Bebb; in that work $\bar{\omega}_v$ was taken as the ionization energy. Consequently, the absorption cross sections reported there are somewhat too small. For continuous final states the sum over the intermediate states $|a_\mu\rangle$ contains the matrix element $\langle a_f|z^{N-\nu-\mu}|a_\mu\rangle$, where $|a_f\rangle$ and $|a_\mu\rangle$ are both in the continuum; an integration over $|a_\mu\rangle$ must then be performed. This difficulty is not encountered in practice, however, since the dense set of states for $\nu=N-1$ generally contains important "near resonances."

III. HYDROGEN

In this section we turn our attention to detailed calculations of N-photon ionization of atomic hydrogen. Since the hydrogenic wave functions are well known, we expected that rather accurate computations can be performed. The development of realistic computational procedures is emphasized. While the techniques employed are not exact (in the sense of Zernik's treatment[16] of two-photon photoionization of $2S$-metastable atomic hydrogen), they are quite precise. Careful computations serve a twofold purpose: first, atomic hydrogen is of interest in its own right and experiments though difficult may be feasible using atomic-beam techniques. Second, the results of the calculations for atomic hydrogen aid the establishment of reasonable approximations for more complicated atoms.

1. Nth-Order Transition Rate for Hydrogen

We now evaluate the Nth-order matrix element defined in Eq. (24) for hydrogen. The positive energy continuum states are formed from eigensolutions common to H_e, $|\mathbf{l}|^2$, and l_z where H_e is the Hamiltonian of the unperturbed atom and $\mathbf{l}$ is the angular-momentum operator. These wave functions will be denoted $|k,l,m\rangle$. The hydrogenic final state is given by the partial-wave expansion[26]

$$|a_f\rangle=|\mathbf{k}\rangle=4\pi\sum_{l=0}^{\infty}\sum_{m=-l}^{l} i^l e^{i\eta_l} R_l^c(\gamma,kr) \times Y_l^m(\theta,\phi)Y_l^{m*}(\theta_k,\phi_k) \quad (33)$$

$$=4\pi\sum_{l=0}^{\infty}\sum_{m=-l}^{l} i^l e^{i\eta_l}|k,l,m\rangle Y_l^{m*}(\theta_k,\phi_k), \quad (34a)$$

where $\gamma=1/ka$,

$$|k,l,m\rangle=R_l^c(\gamma,kr)Y_l^m(\theta,\phi), \quad (34b)$$

$$R_l^c(\gamma,kr)=N_l^c(\gamma)(2kr)^l \times e^{-ikr}F(l+1+i\gamma|2l+2|2ikr), \quad (34c)$$

$$N_l^c(\gamma)=|\Gamma(l+1-i\gamma)|e^{\pi\gamma/2}/(2l+1)!,$$

and finally,

$$\eta_l=\arg\Gamma(l+1-i\gamma). \quad (34d)$$

These wave functions have been treated at length by several authors.[31]

Using the partial-wave expansion (33), the Nth-order matrix element becomes

$$\langle\mathbf{k}|\tau^N|a_g\rangle=4\pi\sum_{l=0}^{\infty}\sum_{m=-l}^{l} i^l e^{i\eta_l}Y_l^m(\theta_k,\phi_k) \times\langle k,l,m|\tau^N|n_g,l_g,m_g\rangle, \quad (35)$$

where $|n_g,l_g,m_g\rangle$ denotes a "hydrogenic" ground state. Since we have chosen our coordinates such that τ^N depends only on z (not x or y), $m=m_g$ in the final state, $|k,l,m_g\rangle$. With this simplification the absolute magnitude of the matrix element squared is given by

$$|\langle\mathbf{k}|\tau^N|n_g,l_g\rangle|^2 =(4\pi)^2\sum_{l=0}^{\infty}\sum_{l'=0}^{\infty}(-i)^l e^{-i\eta_l}(i)^{l'}e^{i\eta_{l'}}Y_l^m(\theta_k,\phi_k) \times Y_{l'}^{m*}(\theta_k,\phi_k)\langle n_g,l_g|\tau^N|k,l'\rangle\langle k,l|\tau^N|n_g,l_g\rangle. \quad (36)$$

The magnetic quantum number m has been suppressed in Eq. (36). Since we are interested in the total ionization rate, we integrate (36) over all angles assumed by $\mathbf{k}$, i.e., over $d\Omega_k$. Using the orthogonality relations for the spherical harmonics, $Y_l^m(\theta_k,\phi_k)$, we find

$$\int d\Omega_k|\langle\mathbf{k}|\tau^N|n_g,l_g\rangle|^2=(4\pi)^2\sum_{l=0}^{\infty}|\langle k,l|\tau^N|n_g,l_g\rangle|^2. \quad (37)$$

For convenience we define

$$|\langle k|\tau^N|n_g,l_g\rangle|^2=\int d\Omega_k|\langle\mathbf{k}|\tau^N|n_g,l_g\rangle|^2. \quad (38)$$

This "integrated" matrix element depends on the wave number k while the "old" matrix element depends on the wave vector $\mathbf{k}$.

The total transition rate can now be written from Eqs. (17) and (18)

$$w_{f,g}^{(N)}=\frac{m/\hbar}{(2\pi)^2}(2\pi\alpha F\omega)^N|\langle k|\tau^N|n_g,l_g\rangle|^2 k. \quad (39)$$

[31] W. Gordon, Z. Physik 48, 180 (1928); Ann. Physik 2, 1013 (1929); A. Sommerfeld and G. Schur, *ibid.* 4, 409 (1930); N. F. Mott and H. S. W. Massey, *The Theory of Atomic Collisions* (Oxford University Press, New York, 1952); and H. A. Bethe and E. Salpeter, *Quantum Theory of One and Two Electron Atoms* (Academic Press Inc., New York, 1957). For a more recent and complete account, see Ref. 26.

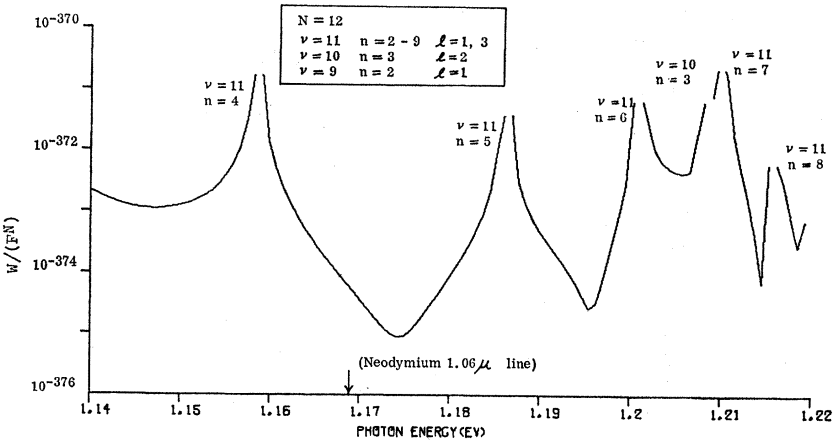

FIG. 2. Dispersion for the 12-photon ionization rate of hydrogen. This is reproduced directly from the digital plotter output as are the subsequent dispersion curves. The dispersion curves are cut off near the resonant energies for $|\hbar(\omega_{n',n_g}-\nu\omega)|<\Delta(\hbar\omega)/200$, where $\Delta(\hbar\omega)$ is the range of photon energies spanned in the figure. To find the transition rate at resonance appropriate to a width γ multiply the maximum value of $w_{f,g}^{(N)}/F^N$ (indicated by the break at each resonance) by $[\nu\Delta(\hbar\omega)/50\gamma]^2$. This gives the value of $w_{f,g}^{(N)}/F^N$ as the resonant denominator $[(\omega_{n',g'}-\nu\omega)^2+\gamma^2/4]$ goes to $[\gamma^2/4]$.

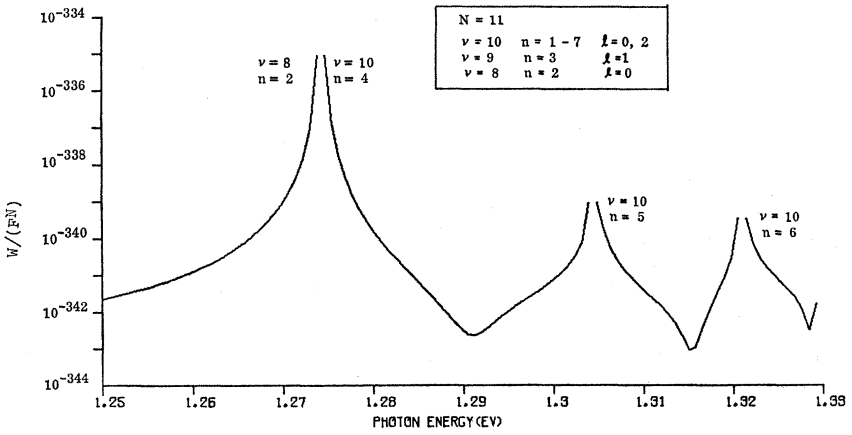

FIG. 3. Dispersion for 11-photon ionization rate. The large peak as $\hbar\omega=1.275$ eV is due to simultaneout resonances in eighth and tenth orders.

The $(N-1)$th order will always be treated as a near resonant state. Using the selection rule $\Delta l=\pm 1$ for dipole matrix elements, the Nth-order matrix element in (39) can be written to display the near resonance

$$
\begin{aligned}
&|\langle k|\tau^N|n_g,l_g\rangle|^2 \\
&=(4\pi)^2\sum_{l=0}^{\infty}|\langle k,l|\tau^N|n_g,l_g\rangle|^2 \\
&=(4\pi)^2\sum_l\left\{\left|\sum_n\frac{\langle k,l+1|z|n,l\rangle}{(\omega_{n,n_g}-(N-1)\omega+i\gamma/2)}\right.\right. \\
&\qquad\left.\left.\times\langle n,l|\tau^{N-1}|n_g,l_g\rangle\right|^2+|\text{term in } l-1|^2\right\}, \quad (40)
\end{aligned}
$$

where the values assumed by l are determined by the nonvanishing contributions of $\langle n,l|\tau^{N-1}|n_g,l_g\rangle$. For convenience the sum over l is referenced to the (N−1)th intermediate state.

Formally, the sum over the principal quantum number n spans the complete set of electronic states, discrete plus continuum. However, because $(N-1)\omega$ typically falls in a spectral region where the states are relatively dense (see Fig. 1), it is reasonable to expect a near resonance for at least one of the values of n (or perhaps several values of n). Hence, only a small number of states together make the dominant contribution to the sum over n, and we can approximate (40) by taking only those states with energies near $(N-1)\hbar\omega$. Since, on the other hand, the states may be closely spaced, $\hbar\omega_{n,n_g}-(N-1)\hbar\omega$ can of course be small over a large range of n. However, it is well known[32] that matrix elements of the form $\langle n,l|z^\nu|n',l'\rangle$ decrease rapidly with increasing n (for $n>n'$) so that the number of significant terms in the sum over n is still limited to about ten for each allowed value of l. In many cases, only one term is needed to obtain a good approximation.

2. Computational Formulas for *N*th-Order Hydrogenic Matrix Elements

The calculation of Nth-order matrix elements breaks naturally into two parts; (1) The evaluation of the bound-bound matrix elements $\langle n,l|\tau^\mu|n_g,l_g\rangle$ appearing

[32] H. A. Bethe and E. Salpeter, *Quantum Theory of One and Two Electron Atoms* (Academic Press Inc., New York, 1957).

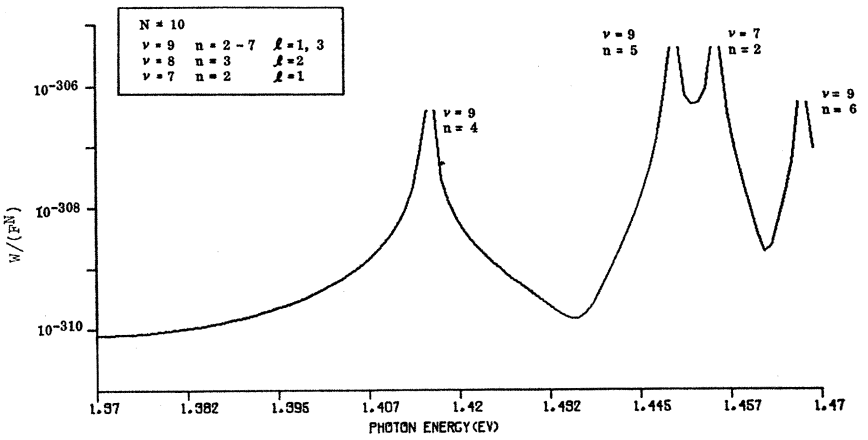

FIG. 4. Dispersion for ten-photon ionization rate.

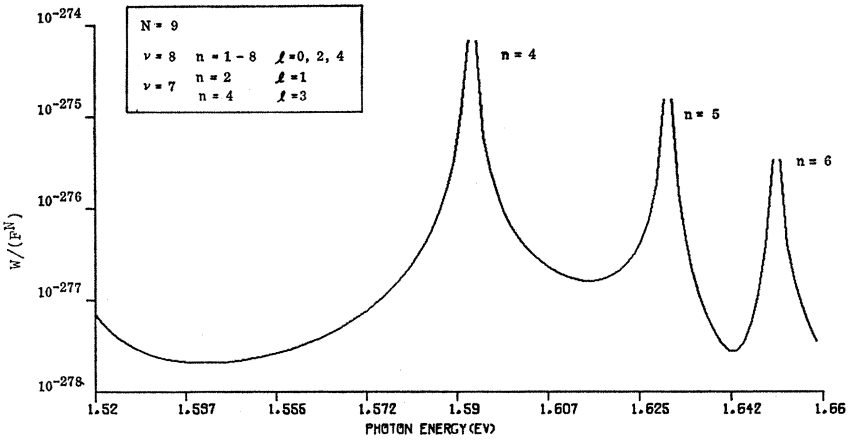

FIG. 5. Dispersion for nine-photon ionization rate.

in Eq. (40), and (2) the evaluation of the sums over the intermediate states containing the near resonances. We have reduced the problem of computing the bound-bound matrix elements to the calculation of an average frequency, $\bar{\omega}_v$ and a single matrix element $\langle n,l|z^u|n_g,l_g\rangle$. The details for computing the average frequency, $\bar{\omega}_v$, for hydrogenic systems are given in Appendix B. We now discuss the remaining "sums" containing the "near-resonant" states and present a computational formula for the hydrogenic Nth-order matrix element. We rewrite Eq. (40) explicitly displaying the frequency dependence and referencing the sum over l to the $(N-1)$th intermediate states (rather than the final states),

$$|\langle k|\tau^N|n_g,l_g\rangle|^2 = (4\pi)^2\sum_l\left\{\left|\sum_n \frac{\langle k,l+1|z|n,l\rangle\langle n,l|z^{N-1}|n_g,l_g\rangle}{(\omega_{n,n_g}-(N-1)\omega)\prod_{\nu=1}^{N-2}(\bar{\omega}_\nu-\nu\omega)}\right|^2 + |\text{term in } (l-1)|^2\right\}. \quad (41)$$

To account for the possible occurrence of near resonances, we sum over n(and all allowed l) up to some maximum, $n_{\max}$. The remaining terms can be approximated in analogy with (B6). We define a new average frequency Ω and approximate (41) by

$$|\langle k|\tau^N|n_g,l_g\rangle|^2 = (4\pi)^2\sum_l\left\{\left|\sum_{n=1}^{n_{\max}} \frac{\langle k,l+1|z|n,l\rangle\langle n,l|z^{N-1}|n_g,l_g\rangle}{(\omega_{n,n_g}-(N-1)\omega)\prod_{\nu=1}^{N-2}(\bar{\omega}_\nu-\nu\omega)} + \frac{\langle k,l+1|z^N|n_g,l_g\rangle - \sum_{n=1}^{n_{\max}}\langle k,l+1|z|n,l\rangle\langle n,l|z^{N-1}|n_g,l_g\rangle}{(\Omega-(N-1)\omega)\prod_{\nu=1}^{N-2}(\bar{\omega}_\nu-\nu\omega)}\right|^2 + |\text{term in } (l-1)|^2\right\}. \quad (42)$$

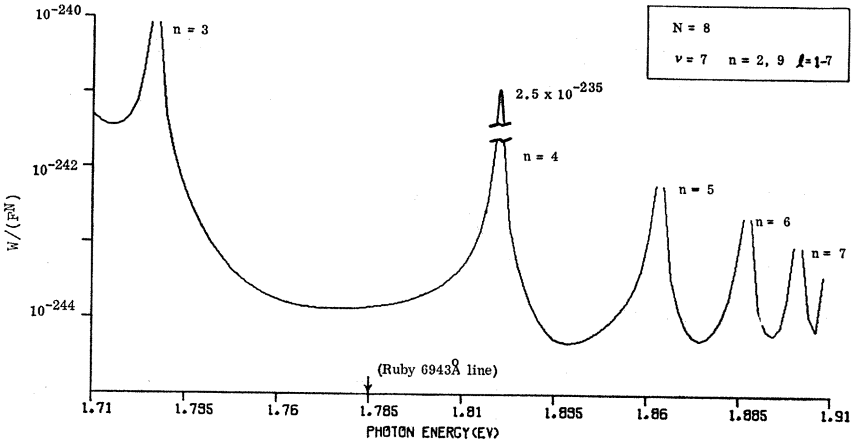

FIG. 6. Dispersion for eight-photon ionization rate. The resonant transition rate at $\hbar\omega = 1.82$ eV (appropriate to a linewidth $\gamma/2 = 10^{-5}$ eV) is indicated. See caption of Fig. 2.

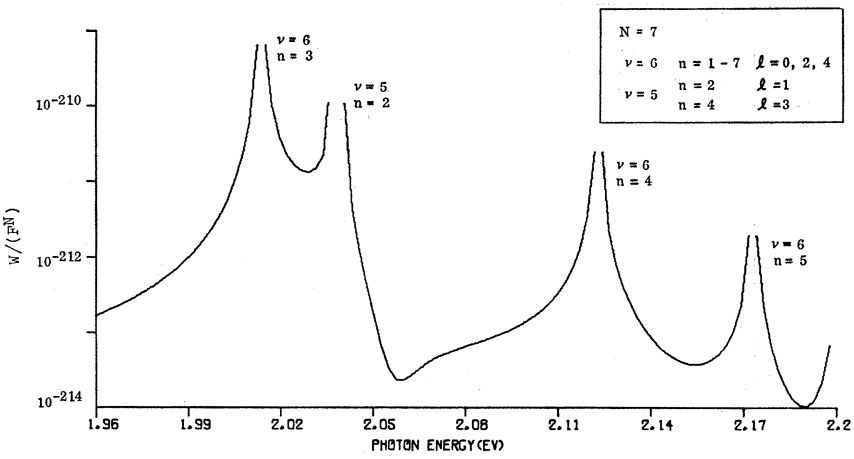

FIG. 7. Dispersion for seven-photon ionization rate.

The average frequency Ω, though not easily calculated, can be reasonably estimated. The term involving Ω represents a sum over the discrete states near the ionization edge together with the continuum states; Ω is the average frequency appropriate to these states. The dominant contribution from the continuum states occurs in a region 1–3 eV above the ionization edge. The energies of the discrete states are near $\hbar\omega_I$. Hence, we expect $\hbar\Omega$ to be near $\hbar\omega_I$.

Choosing $\Omega = 1.2\omega_I$ gives good agreement with Zernik's[16] results for $2S-H$ (second-order photoionization) and ensures that $[\Omega-(N-1)\omega]$ will not become small introducing an artificial resonance behavior. The results are not critically dependent on the choice of Ω since the term involved normally represents only a small contribution to the matrix element.

3. Numerical Results

A FORTRAN computer program was written to evaluate the Nth-transition rate. The main program computes the Nth-order matrix element (42) (using several subroutines to calculate the various radial and angular integrals) and then calculates the transition rate from Eq. (39). The ground-state and intermediate-state quantum numbers and energies, the order N, the number of orders containing near resonances, and the average energies $\hbar\bar{\omega}_\nu$ and $\hbar\Omega$ are supplied as input. The output from the IBM 7074, $w_{f,g}^{(N)}$ and $\hbar\omega$, is written on magnetic tape which is used as input to a Calcomp digital plotter. The digital plotter draws the transition rate as a function of photon energy. The dispersion curves reproduced in this work are taken directly from the digital plotter output [the label $W/(F^N)$ on the ordinate should be read as $w_{f,g}^{(N)}/F^N$].

The Nth-order photoionization transition rates in hydrogen have been calculated for photon energies ranging from 1.14 to 13.4 eV corresponding to the simultaneous absorption of from twelve photons to two photons, respectively. The results are given in Figs. 2 through 13. The figures are ordered with increasing photon energy starting at 1.14 eV ($N=12$). The resonance states and the order ν of the intermediate resonances are indicated, i.e., the resonance in Fig. 2 denoted by $\nu=11$ and $n=4$ corresponds to a small energy denominator $\hbar(\omega_{4,1}-11\omega)$. The states explicitly summed over in each order ν are shown in the inset with the re-

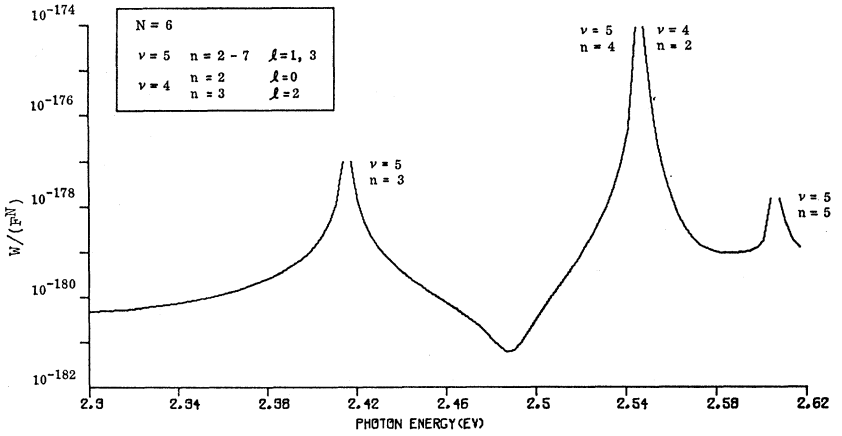

FIG. 8. Dispersion for six-photon ionization rate. The large peak near 2.55 eV arises from resonances occurring simultaneously in fourth and fifth orders. Note that the second harmonic of the neodymium 1.06 line falls near 2.34 eV.

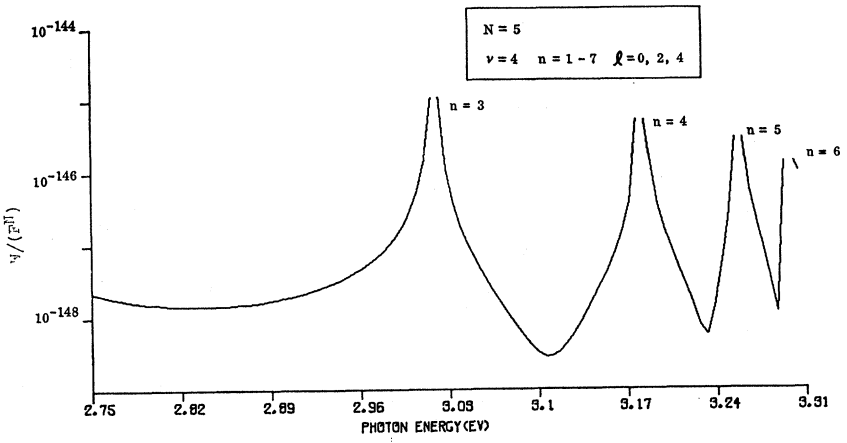

FIG. 9. Dispersion for five-photon ionization rate.

maining states being incorporated through the agency of the average energy $\hbar\Omega = 1.2\hbar\omega_I$. The lower order sums not involving near resonances are approximated by "collapsing" over the average energy 10.2 eV [see Eq. (42)].

Atomic hydrogen ionizes with the absorption of eight ruby quanta (1.785 eV). The dispersion for the 8th order transition rate is given in Fig. 6. It will be seen that seven ruby photon energies fall between the $n=3$ and $n=4$ atomic levels. Increasing the photon energy to ~ 1.82 eV makes $7\hbar\omega$ resonant with the $n=4$ state. We have indicated the corresponding transition rate ($w_{f,g}^{(N)} = 2.5\times 10^{-235} F^8$ sec^{-1}/atom) appropriate to a linewidth of $\frac{1}{2}\gamma = 10^{-5}$ eV.

The dispersion curves show several interesting "coincidences." Referring to Fig. 2, we note that near resonances occur in two separate orders, $\nu = 11$ and 10, at nearly the same photon energy, $\hbar\omega = 1.21$ eV. In fact, the $n=3$ state is a near resonant state for the complete range of photon energies (see Fig. 14) with $|\hbar(\omega_{3,1} - 10\omega)|^2 < 0.47$ for all $\hbar\omega$ within, 1.14 eV $< \hbar\omega < 1.22$ eV; similarly for the $2p$ state, $|\hbar(\omega_{2,1} - 9\omega)|^2 < 0.6$ within the indicated range of photon energies. Hence, we have treated only the $2p$ and $3d$ states as near resonant states ($\nu = 10$ and 11, respectively). The $3s$ state (degenerate with $3d$) is of course also near resonance, but we have neglected its contribution since the matrix element involved is small compared to the $3d$ matrix element (the larger angular-momentum states, in general, make the dominant contribution to the photoionization transition rate).

Additional simultaneous resonances occur at $\hbar\omega = 1.275$ eV ($N=11$) and $\hbar\omega = 2.55$ eV ($N=6$) shown in Figs. 3 and 8, respectively. The lower energy "simultaneous resonance" at 1.275 eV, occurring in orders $\nu = 8$ and 10, is particularly interesting because the resonant atomic states are separated by two photon energies (rather than a single photon energy as with the resonance at $\hbar\omega = 2.55$ eV), i.e., $\hbar\omega_{4,2} = 2.549$ eV and $2\hbar\omega = 2.55$ eV while $8\hbar\omega = 10.2$ eV is very nearly resonant with the $2s$ state (see Fig. 14).

In Fig. 13, our calculation of the two-photon ionization transition rate of $2S$ metastable hydrogen is compared with Zernik's[16] "exact" treatment (Zernik's results are indicated by the dashed line). The average energy $\hbar\Omega$ is taken as $1.2\hbar\omega_I$ ($\hbar\omega_I = 3.399$ eV for $2S$ H). The agreement is good with noticeable discrepancies appearing only far from resonances. This, of course, is

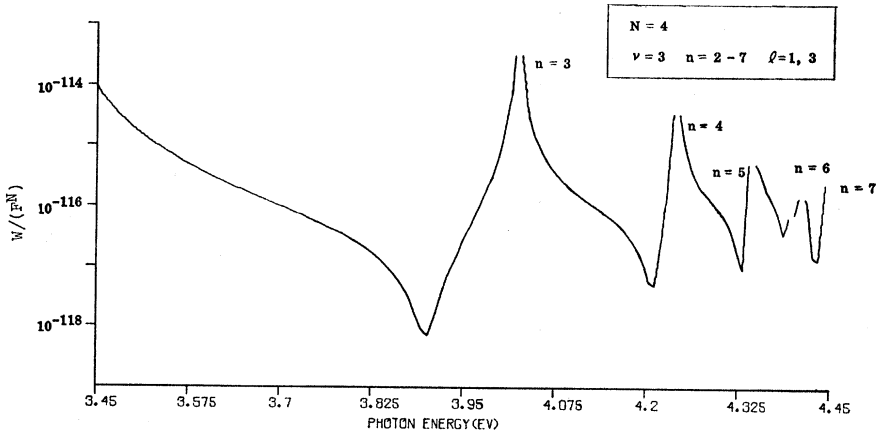

FIG. 10. Dispersion for four-photon ionization rate. The sharp valleys reflect a cancellation effect as the photon energy passes from one resonance to the next. The second harmonic of the ruby 6943-Å line falls near 3.57 eV.

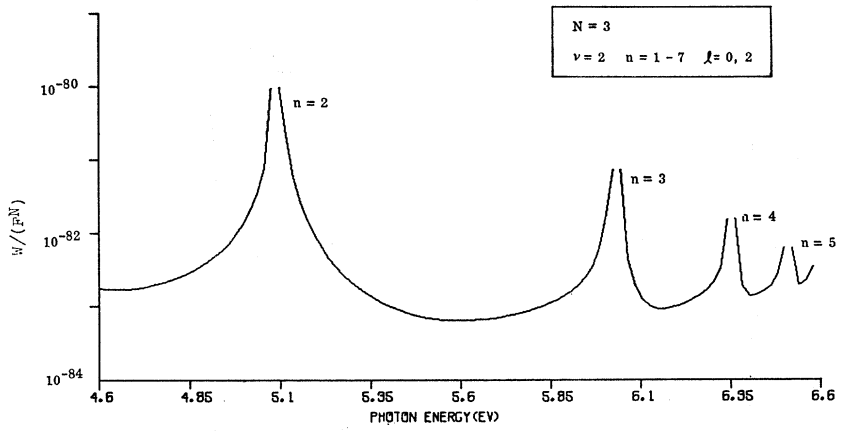

FIG. 11. Dispersion for three-photon ionization rate.

expected since our technique is most accurate for photon energies in near resonance with an atomic state. The ruby photon energy (1.785 eV) is near resonance with the $3p$ hydrogenic state (1.889 eV above the $2s$ state).

IV. RARE GASES

In this section we estimate the N-photon ionization rates of the noble gases Xe, Kr, Ar, Ne, and He, for ruby laser light ($\hbar\omega = 1.785$ eV). These processes require (in the lowest nonvanishing order) the simultaneous absorption of 7, 8, 9, 13, and 14 photons, respectively. Subsection 1 summarizes some minor modifications in the theory and general selection rules. In Subsec. 2 we treat each of the rare gases in turn beginning with He. We give a brief resume of certain features peculiar to each gas, the relevant portions of the spectra and the dispersion for the transition rate in the neighborhood of 1.785 eV.

Most experiments on gas breakdown have been performed over a limited range of atomic densities around $\sim 10^{20}$ atoms cm^{-3} and using a Q-switched ruby laser with $\sim$10-nsec pulse duration, focused into a volume of $\sim 10^{-8}$ cm^{-3}. Taking these values as defining a typical experiment, we find that the initiation flux required to liberate one electron is $\sim 10^{29}$ photons cm^{-2} sec^{-1} for Xe, Kr, and Ar and $\sim 5\times 10^{30}$ photons cm^{-2} sec^{-1} for Ne and He.

1. Theory

The wave functions for the noble gases are approximated by hydrogenic wave functions with the radius of the appropriate Bohr orbit scaled to the atomic radius. Expressing the Nth-order matrix elements in units of $(a_0/Z)^{N+3/2}$, all frequencies in units of electron volts, $\omega(\sim/\text{sec}) = (e/300\hbar)\omega(\text{eV})$, and measuring the wave number k in a_0^{-1}, we can write the integrated transition rate (39) in a convenient numerical form,

$$w_{f,g}^{(N)} = Z^{-3}(1.412\times 10^{12}) \times [0.84564\times 10^{-33} Z^{-2} F\omega_{\text{eV}}]^N |\langle k|r^N|n_g,l_g\rangle|^2 k. \quad (43)$$

The computational form of the matrix element is given by (42). The procedures used for hydrogen are applied unaltered to the rare gases. In analogy with hydrogen, we will take $\hbar\bar{\omega}_v$ as the first excitation energy and $\hbar\Omega = 1.2\hbar\omega_I$. This choice of $\hbar\bar{\omega}_v$ differs from that used by

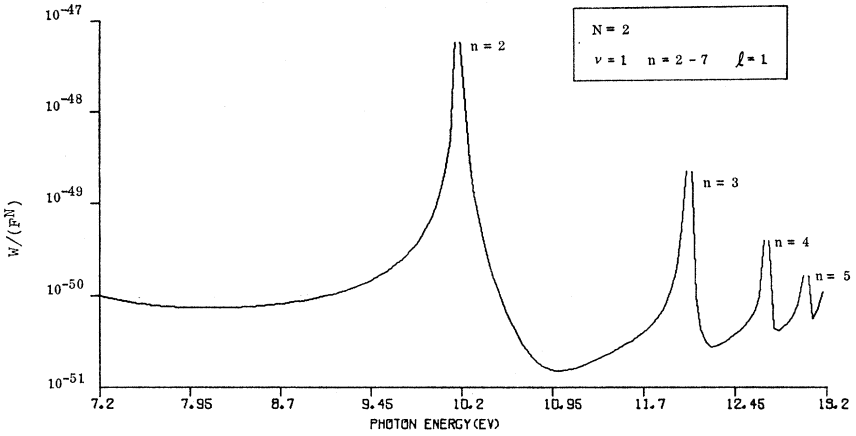

FIG. 12. Dispersion for two-photon ionization rate. The Rydberg series is evident with the peaks corresponding to the hydrogenic spectrum.

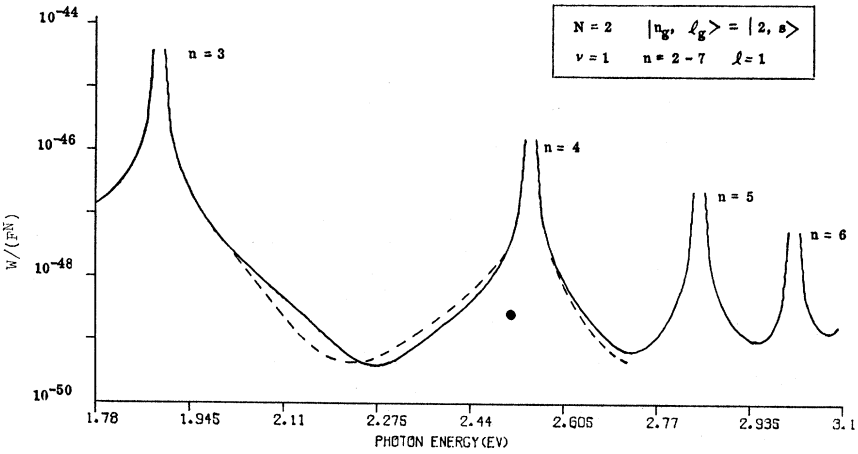

FIG. 13. Dispersion for two-photon ionization rate of 2*S* H comparing the present calculation (solid line) with Zernik's results (dashed line).

Gold and Bebb,[19] where the average energy $\hbar\omega_v$ was taken as the ionization energy, $\hbar\omega_I$.

In contrast to our earlier work, we take explicit account of the intermediate near resonances using the appropriate scaled hydrogenic functions (rather than "collapsing" the matrix element over the resonant denominators) and use scaled Coulomb functions (rather than plane-wave states) to represent the continuum states. The resulting transition rates are larger than those previously reported.

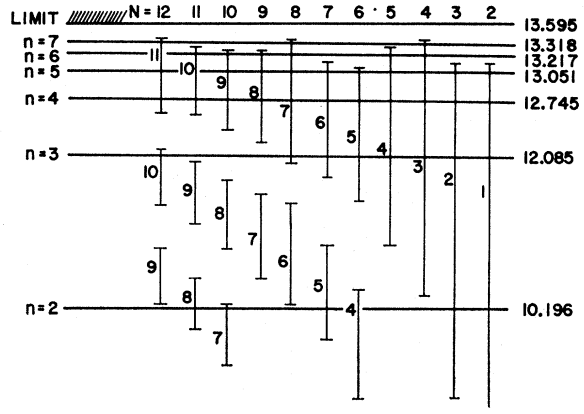

FIG. 14. Resonant energies. The brackets show the range of $\nu\hbar\omega_{eV}$ spanned in the dispersion curves (Figs. 2–12) for hydrogen. *N* specifies the order of the process and the number accompanying each bracket specifies the order ν of the intermediate resonances explicitly "summed on."

Selection rules for an *N*-photon transition are most easily derived by successive applications of the selection rules for one-photon processes. Both (*LS*) and (*jl*) coupling are employed as appropriate. (*jl*) coupling obtains when the "electrostatic interaction is weak compared to the spin-orbit interaction of the parent ion, but is strong compared to the spin coupling of the external electron." In this case we couple the $\mathbf{J}_c$ of the core ion with orbital moment $\mathbf{l}_e$ of the external electron to form a resultant $\mathbf{K}$. The total angular momentum $\mathbf{J}$ is formed by coupling $\mathbf{K}$ to the spin $\mathbf{s}_e$ of the external electron:

$$\mathbf{J}_c=\mathbf{l}_c+\mathbf{s}_c,$$
$$\mathbf{K}=\mathbf{J}_c+\mathbf{l}_e,$$
$$\mathbf{K}+\mathbf{s}_e=\mathbf{J}.$$

TABLE I. Summary of properties of the rare gases. The intermediate states displayed are explicitly summed on according to Eq. (42).

Gas	N	$\hbar\omega_I$ (eV)	$\hbar\tilde{\omega}_v$ (eV)	Atomic radii (angstroms)	Z	ν	Intermediate resonant states LS Designation	jl Designation	Energy
He	14	24.580	21.0	0.93	0.57	13	$1s3p(^1P_1)$	···	23.082
							$4p(^1P_1)$	···	23.737
							$4f(^1F_3)$	···	23.732
							$5f(^1F_3)$	···	24.038
						12	$1s2s(^1S_0)$	···	20.611
Ne	13	21.559	17.0	1.12	0.96	12	$2p^510p(^3P_0)$	$10p\ [\frac{1}{2}]_0$	21.4038
							$11p(^1D_2)$	$11p\ [\frac{3}{2}]_2$	21.4294
						11	$2p^54s(^1P_1)$	$4s'\ [\frac{1}{2}]_1$	19.7749
Ar	9	15.755	11.8	1.54	1.03	8	$3p^55p(^3S_1)$	$5p\ [\frac{1}{2}]_1$	14.46
							$5p(^1D_2)$	$5p\ [\frac{3}{2}]_2$	14.51
Kr	8	13.996	11.3	1.69	1.25	7	$4p^56s(^3P_2)$	$[\frac{3}{2}]_2$	12.3494
							$6s(^3P_1)$	$[\frac{3}{2}]_1$	12.3827
							$4d(^3F_2)$	$[\frac{5}{2}]_2$	12.2552
							$4d(^1F_3)$	$[\frac{5}{2}]_3$	12.2816
							$4d(^3P_1)$	$[\frac{3}{2}]_1$	12.3518
Xe	7	12.127	9.6	1.90	1.4	6	$5p^57p(^3S_1)$	$[\frac{1}{2}]_1$	10.8995

The selection rules in (jl) coupling are

$$\Delta J_c=0,$$
$$\Delta K=0,\pm1,$$
$$\Delta l_e=\pm1,$$

together with $\Delta J=0,\pm1$, and parity change. The levels are specified by $nl[K]_J$ (e.g., the $4s\ ^1P_1$ state of neon written in (jl) notation is $4s[\frac{1}{2}]_1$). Levels belonging to the $^2P_{1/2}$ core are indicated with a primed l value, the unprimed belonging to the $^2P_{3/2}$ core.

Certain of the lower lying states and the $np^5n's$ states can be significantly assigned with LS designations.[33] The higher lying states show (jl) coupling. In Ne, the $2p^53p$ states and the $2p^5ns$ states can be taken as LS-coupled[34]; in Ar the $3p^54p$, $3p^54d$ and the lower $np^5n's$ states are LS coupled,[35] in Kr and Xe, (jl) coupling obtains throughout the spectrum while He, at the other extreme, is LS coupled. The dominant coupling scheme for a given state, of course, affects the selection rules. However, the selection rule $\Delta S=0$ is very weak except in He even for the states listed above as LS coupled. We will adhere to the more familiar LS term designations where meaningful but will resort to (jl) coupling notation where necessary.

In our approximation, the rare-gas wave functions are replaced by scaled hydrogenic functions. Consider for example the one photon excitation of neon to the $2p^54s(^1P_1)$ state; we approximate the dipolar matrix element corresponding to the $2p^6\rightarrow 2p^54s$ transition by $\langle 4s|z|2p\rangle$, where the $|n,l\rangle$ are hydrogenic functions scaled to match the radius of the appropriate Bohr orbit (in this case the $2p$ orbit) to the atomic radius. The scaling is accomplished through the effective charge parameter Z appearing in (43). We should note that the effective Z determined by scaling the orbitals is quite different from the effective Z for energy. Slater[36] has pointed out that the discrepancy is due to screening effects of the core electrons.

2. Numerical Results

We have obtained numerical results for each of the rare gases He, Ne, Ar, Kr, and Xe. They are presented in two forms: the dispersion in the Nth-order transition rate in the neighborhood of 1.785 eV (the ruby-laser photon energy) and the initiation flux required to liberate one electron in a gas concentration of 10^{20} atoms cm^{-3} with a 10-nsec pulse of light in a focal volume of 10^{-8} cm^3 (i.e., the flux, F, required to produce a transition rate per atom of 10^{-4} sec^{-1}).

Some properties of the rare gases needed for the computation of the N-photon ionization rates are summarized in Table I. The order N given in the table is appropriate to ruby laser photons (1.785 eV). The intermediate states explicitly summed on in evaluating (42) are listed together with their energies. Both (LS) and (jl) designations (where appropriate) are given. In the sixth column we give the effective Z scaling parameter.

The energy levels and assignments for the rare gases are taken from the Moore tables.[37]

[33] G. H. Shortley, unpublished material reported in Ref. 37.
[34] A. Gold and R. S. Knox, Phys. Rev. **113**, 834 (1959).
[35] R. S. Knox, Phys. Rev. **110**, 375 (1958).
[36] J. C. Slater, *Quantum Theory of Atomic Structure* (McGraw-Hill Book Company, Inc., New York, 1960), Vol. I, p. 227.
[37] C. E. Moore, *Atomic Energy Levels*, Natl. Bur. Std. (U. S.) Circ. No. 467 (U. S. Government Printing Office, Washington, D. C., 1949).

a. Helium

The relevant portions of the spectrum of He are shown in Fig. 15(a). Integral multiples of the ruby photon energy are marked. It will be seen that the $3p(^1P_1)$ state of He is rather near 13 (1.785 eV) photon energies above the ground state. The dispersion curve for $w_{f,g}^{(N)}/F^N$ given in Fig. 15(b) shows the effect of this near resonance. It is interesting to note that the peak at 1.825 eV [shown in Fig. 15(b)] incorporates two nearly degenerate states, $4p(^1P_1)$ at 23.737 eV and $4f(^1F_3)$ at 23.732 eV.

b. Neon

Neon is of particular experimental interest because of a very near resonance of $12\hbar\omega$ ($=21.4200$ eV for $\hbar\omega=1.785$ eV) with the $11p(^1D_2)$ state at 21.4294 eV above the ground state [see Fig. 16(a)]. Under ideal circumstances it may be possible to observe this resonance, shown in Fig. 16(b), with presently available Q-spoiled ruby lasers. The resonance is centered at 6940.6 Å (1.7858 eV) which corresponds to the wavelength of a ruby cooled to $\sim$250°K. The initiation flux at resonance ($\sim5\times10^{29}$ photons cm^{-2} sec^{-1}) is reduced by a factor of 7 from that at 6943.5 Å (the ruby wavelength at room temperature).

A more detailed investigation of the spectrum of neon reveals a total of eight even parity states between 21.3908 eV and the ionization edge.[37] Six arise from the $2p^5 10p$ configuration and two from the $2p^5 11p$ configuration. They are

$2p^5 10p$	$^3S_1$	$[\frac{1}{2}]_1$	21.3981 eV
	$^3D_3$, $^3D_2$	$[\frac{5}{2}]_{3,2}$	21.3986 eV
	$^3D_1$, $^1D_2$	$[\frac{3}{2}]_{1,2}$	21.3995 eV
	$^3P_0$	$[\frac{1}{2}]_0$	21.4038 eV

and

$2p^5 11p$	$^3D_1$, $^1D_2$	$[\frac{3}{2}]_{1,2}$	21.4294 eV.

All of the states listed possess first-order nonvanishing matrix elements to the $4s[\frac{3}{2}]_1$ (i.e., the $4s^3P_1$ state) except the $10p[\frac{5}{2}]_3$ state which violates the selection rule $\Delta J=0, \pm1$. The $10p[\frac{5}{2}]_3$ state couples to $4s[\frac{3}{2}]_2$. We have taken the $4s^3P_{1,2}$ (or $4s[\frac{3}{2}]_{1,2}$) states as near resonant in eleventh order [the $4s^1P_1$ and $^3P_0$ states violate $\Delta J_c=0$ in the (jl) coupling scheme where they are specified as $4s'[\frac{1}{2}]_{1,0}$].

c. Argon

Argon, krypton, and xenon all show comparable initiation fluxes ($\sim5\times10^{28}$ photons cm^{-2} sec^{-1}) for ruby-laser light and a density of $\sim10^{20}$ atoms cm^{-3}. Referring to the spectrum of Ar [Fig. 17(a)], we see that the $3p^5 4s$ states at 11.5 eV are the first excitation states. We have taken $\hbar\bar{\omega}_v=11.8$ eV. Nine 1.785-eV photons are required to liberate an electron in Ar aided by a reasonably near resonance occurring in eighth order involving the $5p$ excited states. All of the S and D states in the $3p^5 5p$ configuration possess nonvanishing eighth-order matrix elements to the ground state $3p^6\ ^1S_0$ while the P states are probably coupled somewhat more weakly to $^1S_0$.[38] We have approximated the $5p\ ^3S_1$, $5p\ ^3D$, and $5p\ ^1D$ states with two (rather than five) hydrogenic $5p$ functions taking the energies as 14.46 and 14.51 eV, respectively [compare the energies given in Fig. 17(a)]. Hence, the transition rate is believed to be conservatively estimated. The peaks (valleys) in the dispersion curve for the transition rate (flux) shown in Figs. 17(b) and 17(c) are due to the resonances as $8\hbar\omega$ approaches 14.46 and 14.51 eV, respectively.

d. Krypton

Krypton ionizes with the absorption of eight ruby laser quanta through the agency of a near resonance in seventh order with several closely spaced $4d$ and $6s$ levels around 12.4 eV [see Fig. 18(a)]. The transition rate (initiation flux) for Kr is unusually large (small) due probably to the presence of $4d$ near resonant intermediate states which have the same principal quantum number $n(=4)$ as the ground state. The dispersion curve for the transition rate is carried through these resonances in Fig. 18(b) with the lower energy ($\hbar\omega=1.784$) peak arising from the two nearly degenerate levels $6s[\frac{3}{2}]_2$ and $4d[\frac{3}{2}]_1$ and the higher energy ($\hbar\omega\sim1.766$) peak arising from the $6s[\frac{3}{2}]_1$ level.

As evidenced by the pair structure apparent in the spectrum, Kr is (jl) coupled. The resonant $4d$ and $6s$ levels indicated in Fig. 18(a) belong to the $^2P_{3/2}$ core. The $4d'$ and $6s'$ levels belonging to the $^2P_{1/2}$ core lie above 12.8 eV while the remaining $4d$ states lie below the 12.2 eV. We have included only the states (falling between 12.3 and 12.8 eV) listed in Table I in the computation of the transition rates. The sixth-order near resonance seen in Fig. 18(a) is illusory since the $4p^5 5s$ states are odd parity states. The average energy $\hbar\bar{\omega}_v$ has been set (above the $5s$ states) at 11.3 eV to avoid introducing an artificial resonance.

e. Xenon

The relevant portions of the spectrum of Xe are shown in Fig. 19(a). It will be seen that the $5p^5 7p$ even-parity states lie approximately 6 ruby photon energies above the ground state while $5\hbar\omega$ falls between the $6s$ and $6s'$ "pairs." We have incorporated only the lowest $7p$ state as a near resonant state in sixth-order collapsing over the average energy $\hbar\bar{\omega}_v=9.6$ eV in the lower orders. The dispersion curve for the seventh-order photoionization is shown in Fig. 19(b).

The transition rate for Xe (and the other rare gases) has been computed in several different approximations. In addition to the calculation outlined above, we have computed the transition rate treating both $\nu=6$ and 5 as containing near resonances as well as increasing the

[38] See, for example, A. Pery-Thorne and J. E. Chamberline, Proc. Phys. Soc. 82, 133 (1963) and references quoted therein.

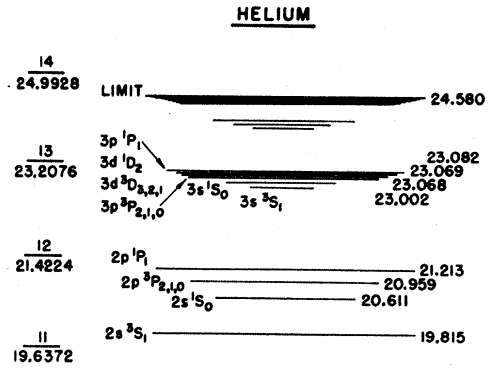

(a)

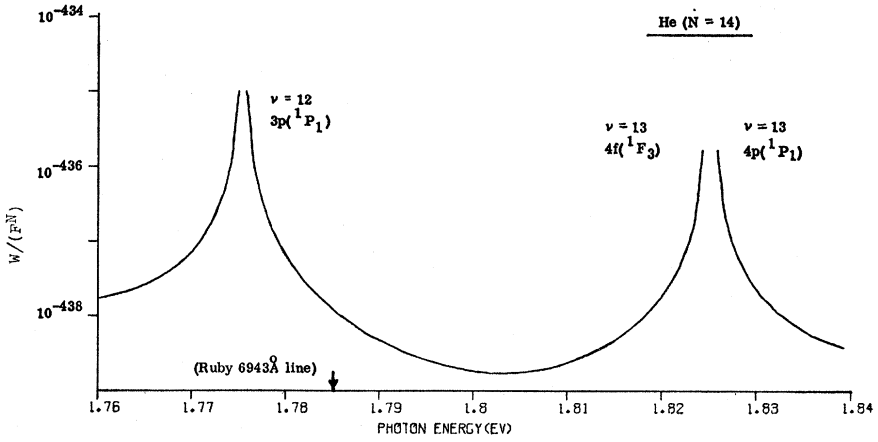

(b)

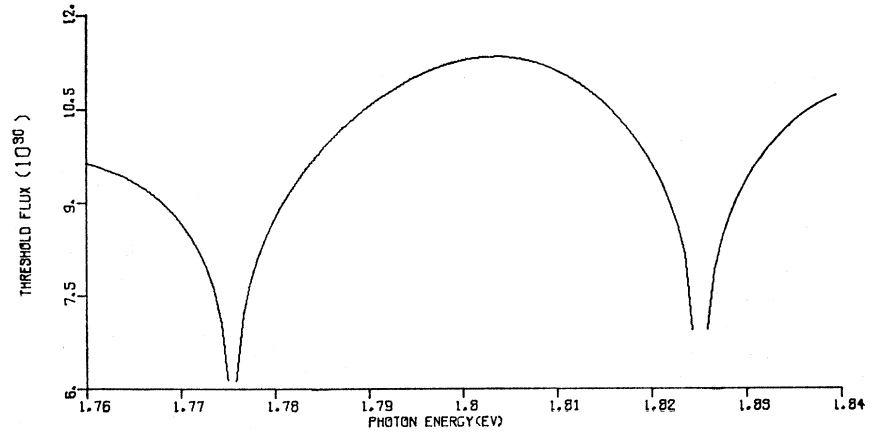

(c)

FIG. 15. Fourteen-photon ionization of He. (a) Relevant portion of the spectrum of He with integral multiples of the ruby photon energy (1.7852 eV) indicated by the left-hand scale. (b) Dispersion for the fourteenth-order transition rate in the neighborhood of the ruby photon energy. (c) Threshold flux for an atomic density of 10^{20} atoms cm^{-3} and a 10 nsec pulse focused into a volume of 10^{-8} cm^3.

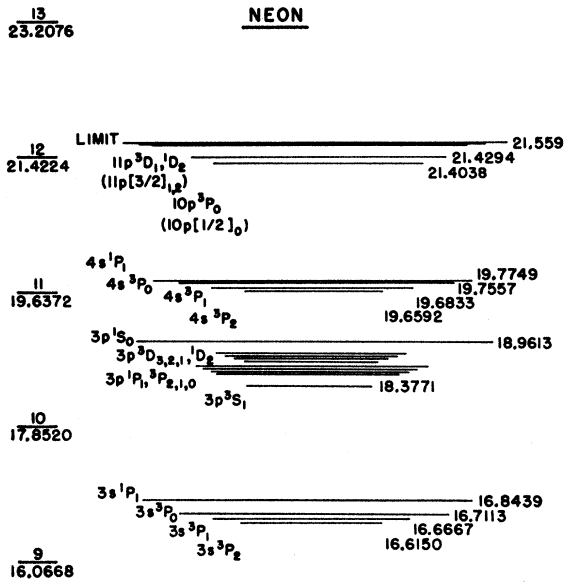

(a)

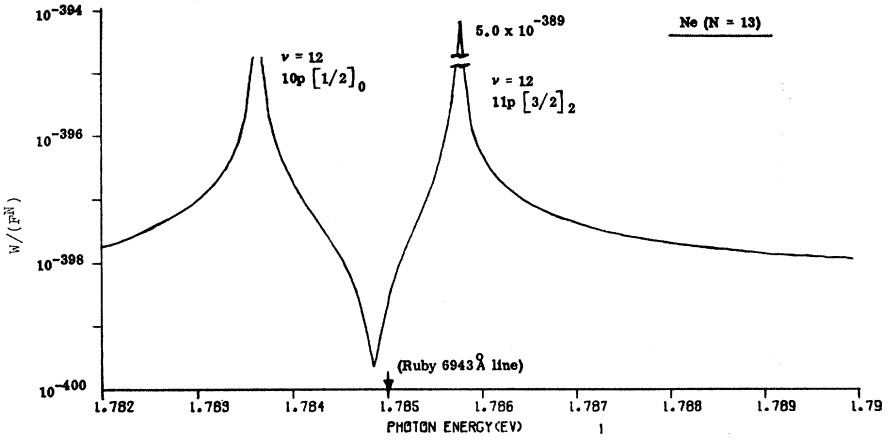

(b)

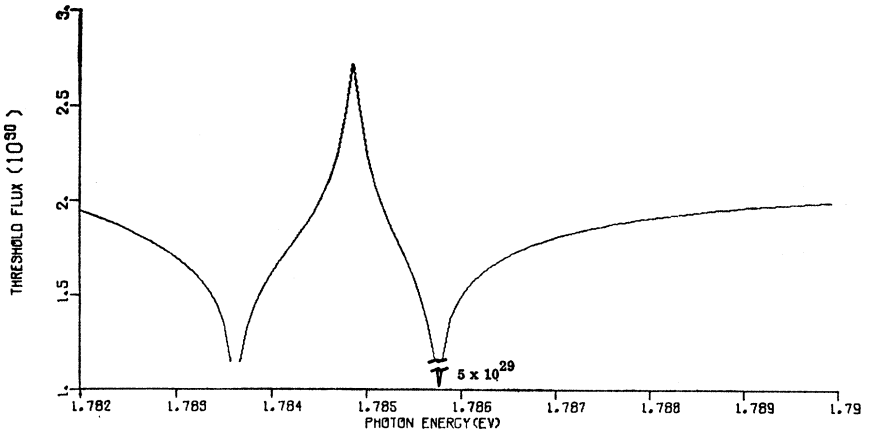

(c)

FIG. 16. Thirteen-photon ionization of Ne. (a) Relevant portion of the spectrum. (b) Dispersion for the thirteenth-order transition rate. The transition rate at the $\hbar\omega = 1.7858$ eV resonance is appropriate to a width $\gamma/2 = 10^{-5}$ eV. (c) Threshold flux for Ne.

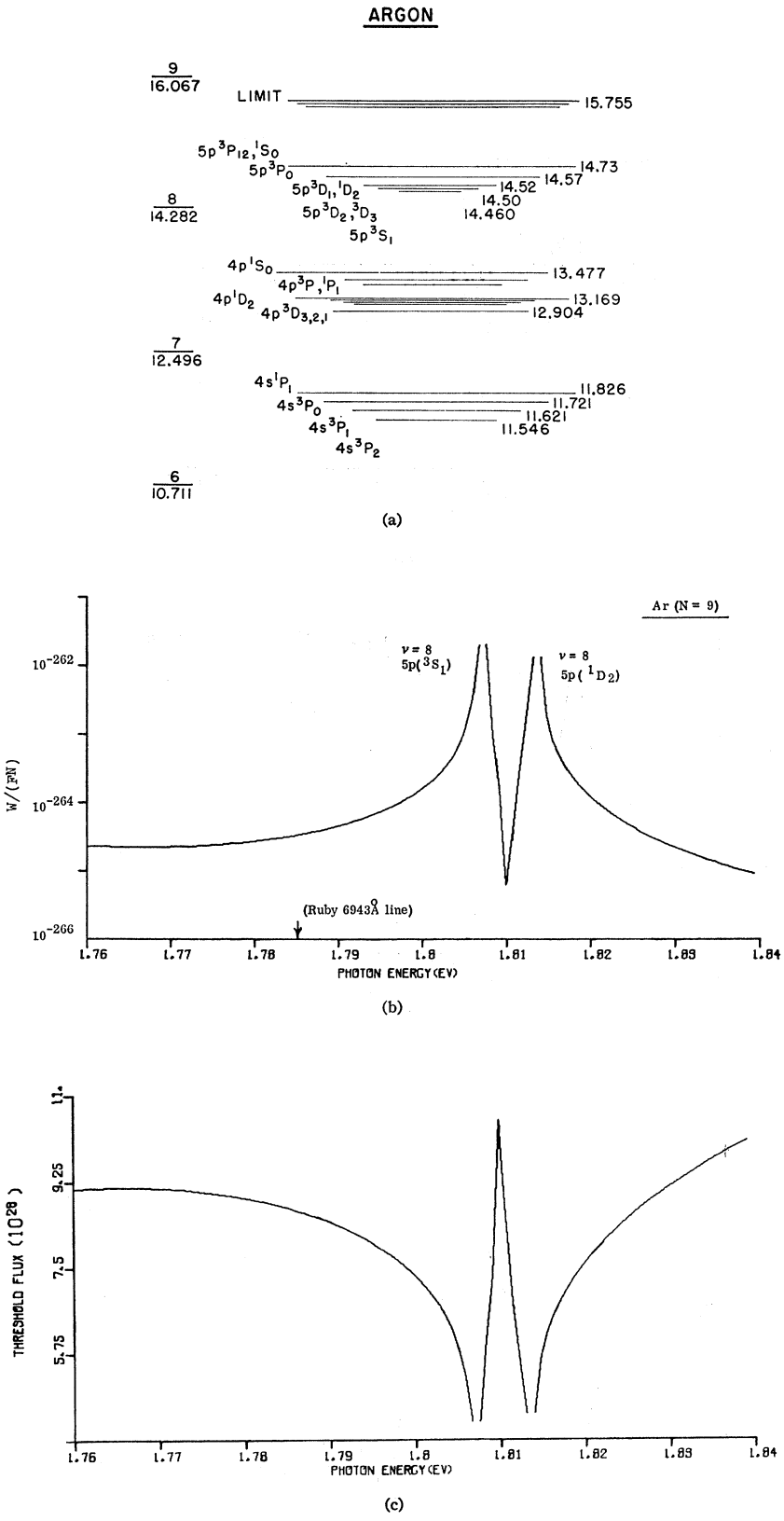

FIG. 17. Nine-photon ionization of Ar. (a) Relevant portion of the spectrum. (b) Dispersion for the ninth-order transition rate. The four D states of the $5p$ configuration (shown in a) have been approximated by a single hydrogenic $5p$ state at 14.51 eV. (c) Threshold flux for Ar.

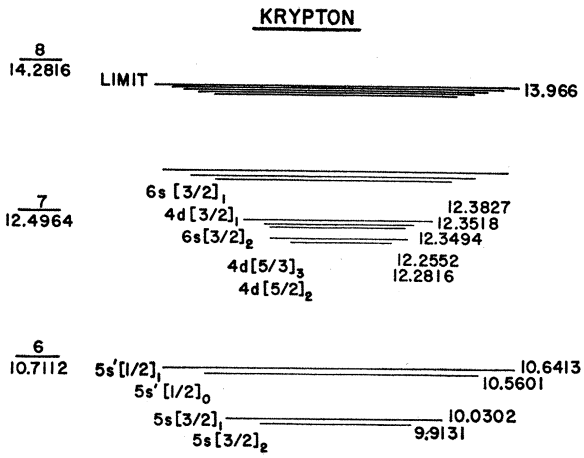

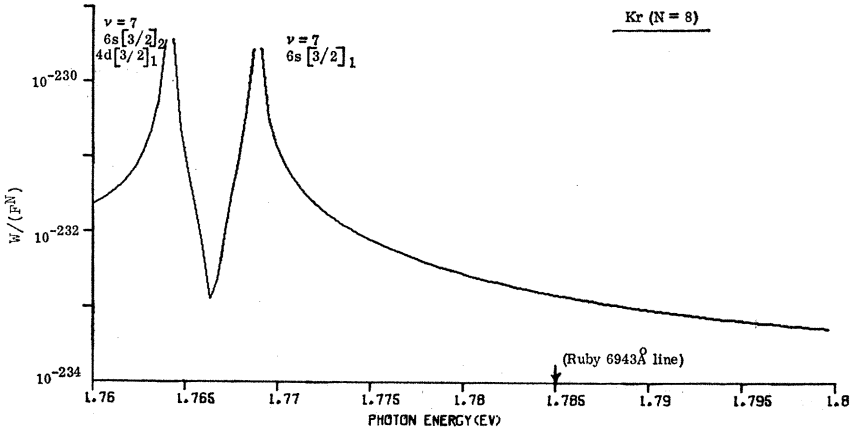

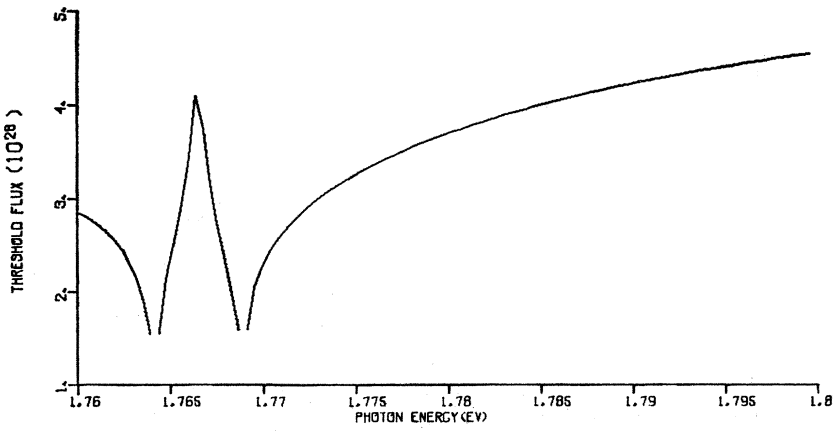

FIG. 18. Eight-photon ionization of Kr. (a) Relevant portion of the spectrum. (b) Dispersion for the eighth-order ionization rate. (c) Threshold flux for Kr.

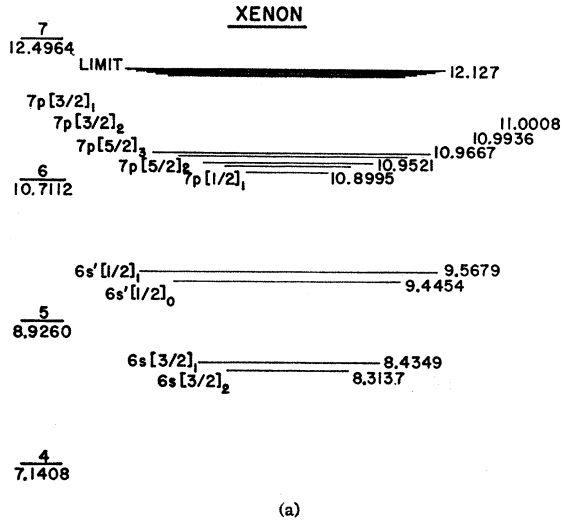

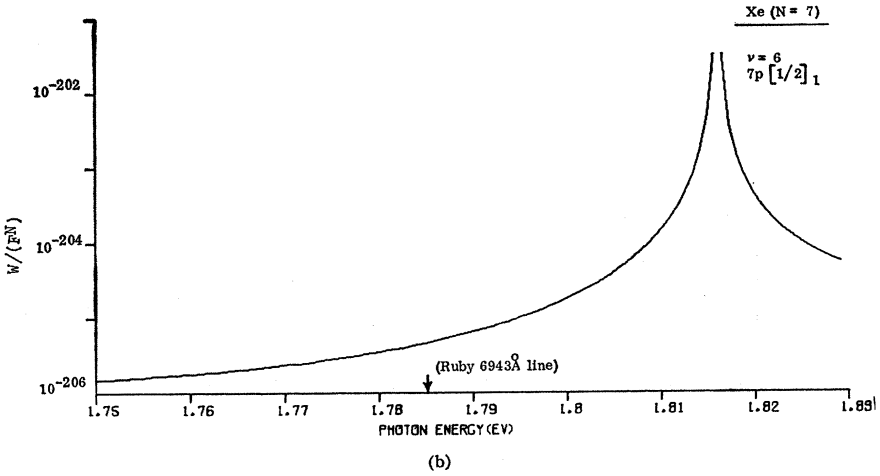

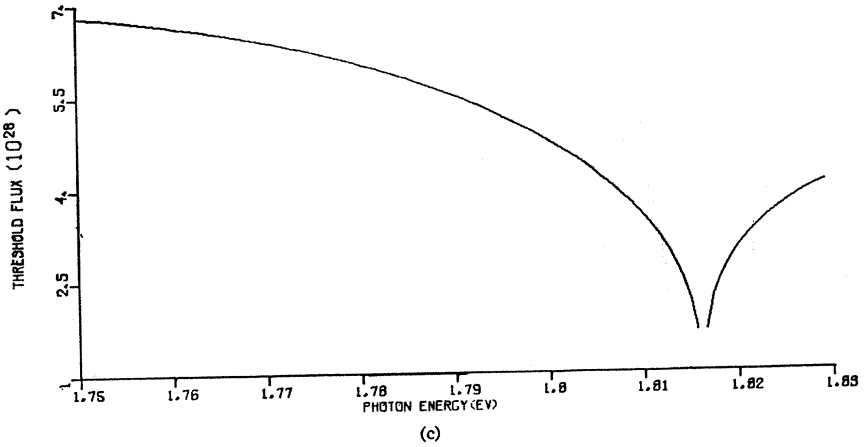

FIG. 19. Seven-photon ionization of Xe. (a) Relevant portion of the spectrum. (b) Dispersion for the seventh-order transition rate. (c) Threshold flux for Xe.

number of $7p$ states explicitly summed on. While these calculations are not detailed here, we stress that the different situations lead to consistent answers insuring that the results are not an artifact of a particular approximation.

V. DISCUSSION

What is the role of multiple-photon ionization in the optical breakdown of gases? The breakdown, occurring in the focal region of a Q-spoiled ruby (or neodymium) laser, is conveniently divided into three stages: (1) initiation, (2) growth, and (3) recombination. Our results indicate that direct multiple-photon ionization can provide a number of free electrons to initiate the breakdown. After the onset of absorption, additional processes[5] (such as inverse bremsstrahlung) cause the ionization rate to increase rapidly until a large fraction (if not virtually all) of the atoms are ionized, resulting in a very high-density plasma ($\sim 10^{19}$ electrons cm^{-3})[1]. At the termination of the laser pulse, the plasma recombines slowly via reasonably well understood processes.[39]

In Fig. 20, we plot the pressure dependence for the direct multiple-photon ionization of the rare gases. The general trends in the observed pressure dependence for gas breakdown of Ar and He are also indicated. While the data given by Meyerand and Haught,[1] Minck,[2] and Waynant and Ramsey[4] differ in detail, it is clear that the pressure dependence for gas breakdown is much stronger than the weak $N_0^{-1/N}$ predicted for N-photon ionization. Hence, even if direct ionization does provide the initiating electrons in the rare gases, some other process (e.g., inverse bremsstrahlung) determines the threshold for the gross discharge.

However, the weak density dependence will greatly enhance the role of any low ionization potential trace impurities present in the gas in providing initiating

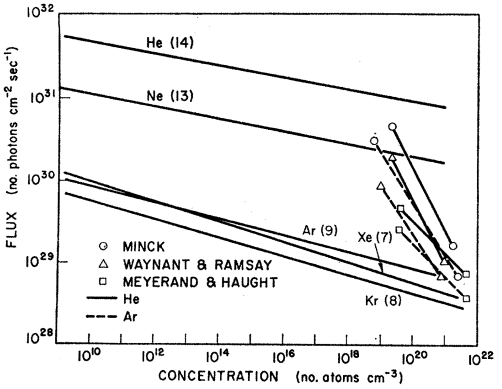

FIG. 20. Atomic density dependence of the N-photon ionization threshold and gas breakdown threshold (see text for a discussion).

[39] See, for example, R. S. Mulliken, Phys. Rev. **136**, A962 (1964) and also W. Finkelnburg and T. Peters, *Handbook der Physik and Spectroscopy* (Springer-Verlag, Berlin, 1955), Vol. II, pp. 28, 79.

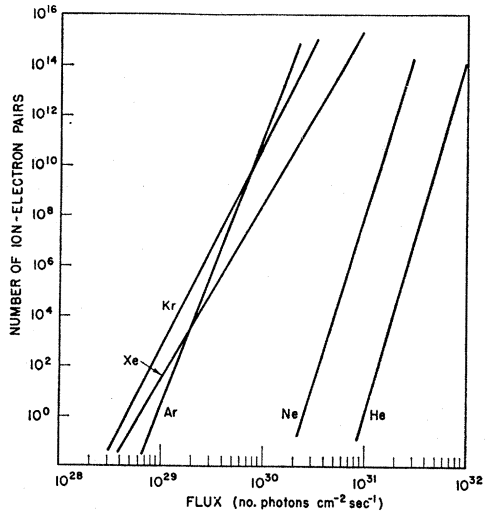

FIG. 21. Number of electrons liberated as a function of the photon flux.

electrons. For example a "hydrogenic model" impurity of ionization potential 7 eV (a reasonable value for many organic molecules) for which $N=4$ will give an initiation flux of $\sim 10^{29}$ photons cm^{-2} sec^{-1} for a concentration of 10^{14} atoms cm^{-3}. An even more severe problem is the presence of "other" rare-gas impurities. A concentration of $\sim 10^{11}$ atoms cm^{-3} of Kr (one part in 10^9) in He would lower the initiation flux to 0.45×10^{30} photons cm^{-2} sec^{-1} as would a concentration of $\sim 10^{13}$ of Xe and Ar.

Figure 21 is a plot of the number of electrons liberated by direct multiple-photon ionization as a function of flux (still assuming the "typical" conditions of a density of 10^{20} atoms cm^{-3} and a 10 nsec pulse from Q-switched ruby laser focused into a volume of 10^{-8} cm^3). The number of ionizations increases very rapidly as F^N. Nth-order photoionization rates are, in fact, proportional to F^N, where F is the instantaneous value of the photon flux. For an optical maser operating in a single mode, we expect the flux (or the occupation number, $n=cF$) to be a well-defined *number* and that[40]

$$\langle F^N\rangle = \langle F\rangle^N \tag{44}$$

where the brackets denote the expectation value. However, for radiation containing more than a single mode, instantaneous fluctuations will cause a different result for $\langle F^N\rangle$. For example, if we consider a large number of modes so that the fluctuations become similar to a thermal source (Gaussian light) we have[40,41]

$$\langle F^N\rangle = N!\langle F\rangle^N. \tag{45}$$

In this extreme, the transition rate is increased by $N!$ over that produced by a *single-mode* laser with the same

[40] L. Mandel and E. Wolf, Rev. Mod. Phys. **37**, 231 (1965).
[41] J. Ducuing and N. Bloembergen, Phys. Rev. **133**, A1493 (1964).

average power. The average flux required to produce a given transition rate is reduced by $(N!)^{-1/N}$.

The radiation from a typical optical-maser source falls somewhere between these two extremes, into the difficult intermediate regime where little is known. Hodara[42] has investigated the distribution for a small number of sinusoidal waves superimposed on Gaussian noise. He found that the deviation from a pure Gaussian distribution decreased rapidly as the number of sinusoidal waves was increased, with the distribution for only five sinusoidal waves plus Gaussian noise approaching very closely a pure Gaussian. In an ordinary ruby laser (as well as a neodymium-glass laser) many different frequencies and spatial modes are observed to be present.[43] It would thus seem that in the absence of detailed information we might reasonably associate a Gaussian distribution with multimode laser light (at least in preference to assuming single-mode operation). In comparing the theory of N-photon ionization with relevant experiments, we must keep in mind that the "effective value" of the flux may be greater than the average measured value by as much as $(N!)^{1/N}$. The theoretical initiation fluxes quoted are, therefore, probably larger than those required in most cases. In fact, it would be of considerable interest to repeat the experiments on gas breakdown utilizing a single-mode laser to determine the effects of fluctuations on higher order processes.

Recently reported experimental techniques can measure higher order multiple-photon ionization transition rates directly. While gas breakdown provides some evidence for N-photon ionization, other effects obscure the process. However, at very low pressures, N-photon ionization dominates. Voronov and Delone[22] have measured the ionization threshold for Xe. They find a "cross section" w/F^7, of $\sim 5\times 10^{-206}$, in good agreement with the value 4×10^{-206} predicted from theory.

ACKNOWLEDGMENT

The authors wish to express their gratitude to Professor M. M. Hercher for many stimulating discussions, especially with regard to experimental aspects of the problem.

APPENDIX A: SELECTION RULES

We consider simple methods for evaluating the angular part of the matrix element,

$$\langle n',l',m'|z^\nu|n,l,m\rangle = C_\nu{}^m(l'|l)\langle n',l'|r^\nu|n,l\rangle, \quad \text{(A1)}$$

where

$$C_\nu{}^m(l'|l) = \langle Y_{l'}{}^m|\cos^\nu\theta|Y_l{}^m\rangle. \quad \text{(A2)}$$

The selection rule $m'=m$ is an immediate consequence of our choice of coordinates. Since $\cos\theta$ is proportional to $Y_1{}^0$, we can write

$$\cos^\nu\theta Y_l{}^m(\theta,\phi) = \sum_{l'} C_\nu{}^m(l''|l) Y_{l'}{}^m(\theta,\phi). \quad \text{(A3)}$$

The expansion coefficients $C_\nu{}^m(l''|l)$ are defined by Eq. (A2). The problem of evaluating the angular part of (A1) is just that of determining the expansion coefficients in (A3). For $\nu=1$, Eq. (A3) reduces to the ordinary recursion relation for the spherical harmonics,

$$\cos\theta\, Y_l{}^m = C_1{}^m(l+1|l) Y_{l+1}{}^m + C_1{}^m(l-1|l) Y_{l-1}{}^m, \quad \text{(A4a)}$$

where

$$C_1{}^m(l+1|l) = [(l+m+1)(l-m+1)/(2l+1)(2l+3)]^{1/2} \quad \text{(A4b)}$$

and

$$C_1{}^m(l-1|l) = [(l+m)(l-m)/(2l-1)(2l+1)]^{1/2}. \quad \text{(A4c)}$$

The coefficients (A2) can also be immediately recorded for an s state. Using the well known expansion[44] for $\cos^\nu\theta$ (in terms of the Legendre polynomials) and the relation $Y_l{}^0(\theta) = [(2l+1)/4\pi]^{1/2} P_l(\cos\theta)$ we have,

(a) for even powers of $\cos\theta$, $\nu=2\mu$, $l'=2s$,

$$C_{2\mu}{}^0(2s|0) = \mu!\, 2^s (4s+1)^{1/2}/(\mu-s)! \prod_{t=0}^{s}(2\mu+2t+1), \quad \text{(A5a)}$$

(b) and for odd powers of $\cos\theta$, $\nu=2\mu+1$, $l'=2s+1$,

$$C_{2\mu+1}{}^0(2s+1|0) = \mu!\, 2^s (4s+3)^{1/2}/(\mu-s)! \prod_{t=0}^{s}(2\mu+2t+3), \quad \text{(A5b)}$$

with the additional condition that $C_\nu{}^0(l'|0)=0$ for $l'>\nu$. These formulas evaluate

$$C_\nu{}^0(l'|0) = \langle Y_{l'}{}^0|\cos^\nu\theta|Y_0{}^0\rangle.$$

It is now a straightforward matter to evaluate (A2) for an arbitrary pair of spherical harmonics. Using (A3) we have

$$\cos^\nu\theta = (4\pi)^{1/2} \sum_{\lambda=0}^{\nu} C_\nu{}^0(\lambda|0) Y_\lambda{}^0, \quad \text{(A6)}$$

with the coefficients being given by Eqs. (A5). Forming the matrix element (A2) we get

$$C_\nu{}^m(l'|l) = \langle Y_{l'}{}^m|\cos^\nu\theta|Y_l{}^m\rangle = (4\pi)^{1/2} \sum_{\lambda=0}^{\nu} C_\nu{}^0(\lambda|0)\langle Y_{l'}{}^m|Y_\lambda{}^m|Y_l{}^m\rangle. \quad \text{(A7)}$$

The integral $\langle Y_{l'}{}^m|Y_\lambda{}^0|Y_l{}^m\rangle$ arises in calculating Clebsch-Gordan coefficients and related vector-coupling

[42] H. Hodara, Western Electronic Show and Convention, Paper 17.4, 1964 (unpublished). See also Ref. 40 for a summary of Hodara's paper and additional relevant discussion.

[43] S. L. Ridgway, G. L. Clark, and C. M. York, J. Opt. Soc. Am. 53, 700 (1963).

[44] P. M. Morse and H. Feshbach, *Methods of Theoretical Physics* (McGraw-Hill Book Company, Inc., New York, 1953), Vol. II, p. 1326.

problems. It is given (in terms of the "3j" symbols) by[45]

$$(4\pi)^{1/2}\int Y_{l'}{}^{m}Y_{\lambda}{}^{0}Y_{l}{}^{m}d\Omega$$

$$=(-1)^{m}[(2l'+1)(2\lambda+1)(2l+1)]^{1/2}\times\begin{pmatrix} l' & \lambda & l \\ 0 & 0 & 0\end{pmatrix}\begin{pmatrix} l' & \lambda & l \\ m & 0 & m\end{pmatrix}. \quad \text{(A8)}$$

The selection rules can be inferred from (A7) using the definitions of $C_{\nu}{}^{0}(\lambda|0)$ and the $3j$ symbols.[46]

For ν even

$$l'=l,\ l\pm2,\ l\pm4,\ \cdots,\ l\pm\nu \quad \text{(A9a)}$$

and for ν odd

$$l'=l\pm1,\ l\pm3,\ \cdots,\ l\pm\nu \quad \text{(A9b)}$$

together with $l'\geqslant 0$. Formal evaluation of the nonvanishing angular integrals (A2), however, is unnecessarily complicated.

A simple diagrammatic technique is based on successive applications of the recursion relation (A4a). In Fig. 22, the order ν is plotted along the ordinate and the angular-momentum quantum number l is indicated on the abscissa. Let l denote the initial angular state, $|l,m\rangle$. The "allowed" final states in order ν are determined by the "intersections" occurring along a line drawn through the desired value of ν parallel to the abscissa. The value of the angular integral $C_{\nu}{}^{m}(l'|l)$ is given by a sum of products of $C_1{}^{m}(l\pm1|l)$ determined by the possible "paths" between l and l'. Referring still to Fig. 22, a "path" between l and l' is any line along the diagonal lines shown starting at l and proceeding to l' always in the direction of increasing order, ν; a "path" must not include any negative values of l.

To illustrate the use of the diagram, we calculate $C_3{}^{m}(l+1|l)$. Start at l and follow "path 1" (indicated in Fig. 22) going through the "steps" $\nu=1$, $l'=l+1$, and $\nu=2$, $l'=l+2$, and finally to $\nu=3$, $l'=l+1$. We associate one of the coefficients (A4) with each "step," $C_1{}^{m}(l+1|l)$, $C_1{}^{m}(l+2|l+1)$, and finally $C_1{}^{m}(l+1|l+2)$. Multiplying these three coefficients and adding the appropriate products associated with "path 2" and then "path 3," we obtain the desired result. The bookkeeping is conveniently tabulated below:

Path / ν	1	2	3
1	$C_1{}^{m}(l+1\|l)$	$C_1{}^{m}(l+1\|l)$	$C_1{}^{m}(l-1\|l)$
2	$C_1{}^{m}(l+2\|l+1)$	$C_1{}^{m}(l\|l+1)$	$C_1{}^{m}(l\|l-1)$
3	$C_1{}^{m}(l+1\|l+2)$	$C_1{}^{m}(l+1\|l)$	$C_1{}^{m}(l+1\|l)$

[45] See Ref. 26, Vol. II, p. 1057.

[46] H. B. Bebb, thesis, University of Rochester, 1965 (unpublished).

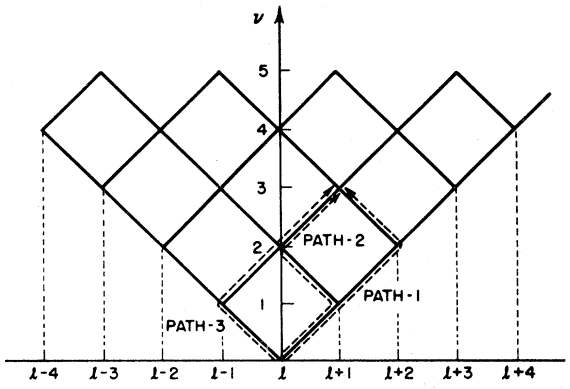

FIG. 22. Diagram for obtaining selection rules and values of $\langle Y_{l'}{}^{m'}|\cos^{\nu}\theta|Y_{l}{}^{m}\rangle$.

To obtain $C_3{}^{m}(l+1|l)$ we multiply vertically (from bottom to top) and sum over the products,

$$C_3{}^{m}(l+1|l)=C_1{}^{m}(l+1|l+2)C_1{}^{m}(l+2|l+1)C_1{}^{m}(l+1|l)+C_1{}^{m}(l+1|l)C_1{}^{m}(l|l+1)C_1{}^{m}(l+1|l)+C_1{}^{m}(l+1|l)C_1{}^{m}(l|l-1)C_1{}^{m}(l-1|l).$$

Note that if $l=0$, "path 3" is not allowed, i.e., $C_1{}^{m}(l-1|l)=0$. The validity of the diagrammatic method for evaluating $C_{\nu}{}^{m}(l'|l)$ is readily established by successive applications of the recursion formula (A4a).

APPENDIX B

Using the concept of an average frequency, $\bar{\omega}_{\nu}$, the μth order bound-bound matrix element can be written,

$$\langle n,l|\tau^{\mu}|n_g,l_g\rangle=\langle n,l|z^{\mu}|n_g,l_g\rangle/\prod_{\lambda=1}^{\mu-1}(\bar{\omega}_{\nu}-\lambda\omega). \quad \text{(B1)}$$

The central problem in the evaluation of (B1) is the computation of the average frequency $\bar{\omega}_{\nu}$ defined by Eqs. (31) and (32). Writing out these definitions explicitly, we have

$$\sum_{n',l'}\frac{\langle n,l|z^{\mu-\lambda}|n',l'\rangle\langle n',l'|z^{\lambda}|n_g,l_g\rangle}{(\omega_{n',n_g}-\lambda\omega)}+\sum_{l'}\int\frac{2}{\pi}k^{2}dk\frac{\langle n,l|z^{\mu-\lambda}|k,l'\rangle\langle k,l'|z^{\lambda}|n_g,l_g\rangle}{(\omega_I+\hbar k^{2}/2m-\lambda\omega)}=\frac{\langle n,l|z^{\mu}|n_g,l_g\rangle}{(\bar{\omega}_{\mu}(\lambda)-\lambda\omega)}, \quad \text{(B2)}$$

with $\bar{\omega}_{\nu}$ defined by

$$\prod_{\lambda=1}^{\mu-1}(\bar{\omega}_{\nu}-\lambda\omega)=\prod_{\lambda=1}^{\mu-1}(\bar{\omega}_{\mu}(\lambda)-\lambda\omega). \quad \text{(B3)}$$

TABLE II. Average energies computed using Eqs. (B4) and (B7). The initial state is taken as $|1,0\rangle$. The first two energies in the last row are missing because of computational difficulties.

State (n,l)	Order	Average energies (eV) $\hbar\omega(1)$	$\hbar\omega(2)$	$\hbar\omega(3)$	$\hbar\omega(4)$	$\hbar\omega(5)$	$\hbar\omega(6)$	$\hbar\omega$ (eV)
		8.44						4.6
2, 0	2	8.52						5.0
		8.63						6.0
3, 0	2	10.38						5.0
3, 2	2	8.19						5.0
		8.49	11.98					3.5
2, 1	3	8.56	11.48					4.0
		8.63	11.00					4.5
4, 3	3	6.74	10.27					4.0
2, 0	4	7.37	10.55	10.10				2.8
4, 0	4	9.82	3.30	4.63				2.8
4, 2	4	7.30	10.72	10.63				2.8
4, 1	7	...	...	9.23	10.55	11.05	12.59	1.785

In (B2), ω_I is the frequency associated with the ionization energy, $\epsilon_I=\hbar\omega_I=13.595$ eV. The factor $2k^2/\pi$ is the density of states appropriate to the continuum eigenstates, $|k,l,m\rangle$ [as contrasted to the density of states, $(2\pi)^{-3}$, appropriate to $|\mathbf{k}\rangle$]. Denoting the left-hand side of (B2) by $A_{n,l^\mu}(\lambda)$, we can solve for $\bar{\omega}_\mu(\lambda)$ obtaining

$$\bar{\omega}_\mu(\lambda)=\lambda\omega+\langle n,l|z^\mu|n_g,l_g\rangle/A_{n,l^\mu}(\lambda). \quad \text{(B4)}$$

Thus, the evaluation of the average frequency hinges on a realistic computation of $A_{n,l^\mu}(\lambda)$.

The general procedure for calculating $A_{n,l^\mu}(\lambda)$ is to sum over a reasonable range n' (say to $n'=18$), and all allowed l', perform the integral over the continuum states directly, and then add a correction term for the states not included ($n'=19$ to ∞). We define

$$B=\sum_{n'=1}^{18}\sum_{l'}\langle n,l|z^{\mu-\lambda}|n',l'\rangle\langle n',l'|z^\lambda|n_g,l_g\rangle + \sum_{l'}\int\frac{2}{\pi}k^2dk\langle n,l|z^{\mu-\lambda}|k,l'\rangle\langle k,l'|z^\lambda|n_g,l_g\rangle. \quad \text{(B5)}$$

To account for the states not included in B, we define a correction term,

$$C=\langle n,l|z^\mu|n_g,l_g\rangle-B. \quad \text{(B6)}$$

Using these definitions, we can write a computational formula for

$$A_{n,l^\mu}(\lambda)=\sum_{n'=1}^{18}\sum_{l'}\frac{\langle n,l|z^{\mu-\lambda}|n',l'\rangle\langle n',l'|z^\lambda|n_g,l_g\rangle}{(\omega_{n',n_g}-\lambda\omega)} + \sum_{l'}\int_\pi^2\frac{-k^2dk\langle n,l|z^{\mu-\lambda}|k,l'\rangle\langle k,l'|z^\lambda|n_g,l_g\rangle}{(\omega_I+\hbar k^2/2m-\lambda\omega)} + C/(\omega_I-\lambda\omega). \quad \text{(B7)}$$

The only approximation contained in (B7) is the replacement of $\omega_{n',n_g}(n'>18)$ by ω_I in the correction term. Since $\hbar(\omega_I-\omega_{n'=19,n_g=1})\sim10^{-4}$ eV, the numerical error is insignificant.

Several typical values of the average energies $\hbar\bar{\omega}(\nu)$ are given in Table II. The word "order" in column two refers to the order μ of the bound-bound matrix element defined in (B1). The numbers tabulated were selected to illustrate the possible range in $\hbar\bar{\omega}(\nu)$, rather than to substantiate $\hbar\omega_\nu=10.2$ as a "universal" average energy (for hydrogen). For example, the average energies for $\langle4,0|\tau^4|1,0\rangle$ fall well below the first excitation energy of hydrogen (10.2 eV) with $\hbar\bar{\omega}(2)=3.30$ eV. This is due to strong coupling to the ground state. Nevertheless, replacing these small energies by $\hbar\bar{\omega}_\nu=10.2$ eV causes little error in the transition rate as the contribution from $\langle4,2|\tau^4|1,0\rangle$ dominates. The average energies appropriate to the eighth-order photo-ionization of hydrogen with ruby laser light are given in the last row (order=7). The first two energies are missing due to computational difficulties in evaluating certain high order bound-free matrix elements.

A FORTRAN computer program was written for the IBM 7074 to evaluate (B4). The initial and final states, the order, and the photon energy are supplied as input. Several subprograms calculate the matrix elements with the main program supplying the selection rules and performing the integrals over k. On the grounds of practicality, we choose to approximate the true average energy with 10.2 eV in our calculations.